Chapter 2: Literature Review

The review of relevant literature is divided into main sections for materials and methods. The section devoted to materials develops an understanding of the chemical variables which influence this study and is further subdivided as follows:

- conventional and ultra-low monol content PPG polyols
- poly(urethane) and poly(urethane-urea) chemistry
- microphase separation of poly(urethane)s and poly(urethane-urea)s
- hydrogen bonding of poly(urethane)s and poly(urethane-urea)s
- development and production of spandex fibers

The section devoted to methods elucidates what information each tool may provide, how it does so, and highlights concerns when using these methods on poly(urethane-urea)s. It is similarly subdivided into sections addressing the primary testing methods used during these investigations:

- Overview of experimental methods
- Small angle x-ray scattering (SAXS)
- Atomic force microscopy (AFM)
- Dynamic mechanical analysis (DMA)
- Differential scanning calorimetry (DSC)
- Wide angle x-ray scattering (WAXS)
- Birefringence
- Infrared linear dichroism (LD)
- Mechanical tensile testing

Section 2-1: Materials - Poly(propylene glycol)

Poly(propylene glycol) has traditionally, since the 1960s, been produced through a base catalyzed process that involves the propoxylation of a starter material that possesses at least two hydroxyls (Figure 2-1). It is essentially a ring-opening polymerization that results, ideally, in a polyol, in this case, PPG. However, there exists a side reaction that ultimately limits the effective use of PPG in high-end elastomeric applications. The base used to catalyze the

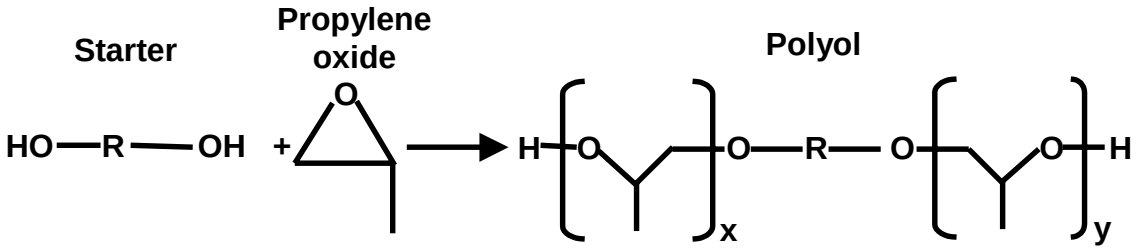

Figure 2-1. Base Catalyzed Production of Poly(propylene glycol).[8]

polymerization, generally KOH, will also catalyze an isomerization of the propylene oxide into an allyl alcohol.[1-3] The allyl alcohol will then act as a monofunctional starter material for the polymerization and will ultimately result in what is termed “monol” (Figure 2-2). The monol, as will be seen when the

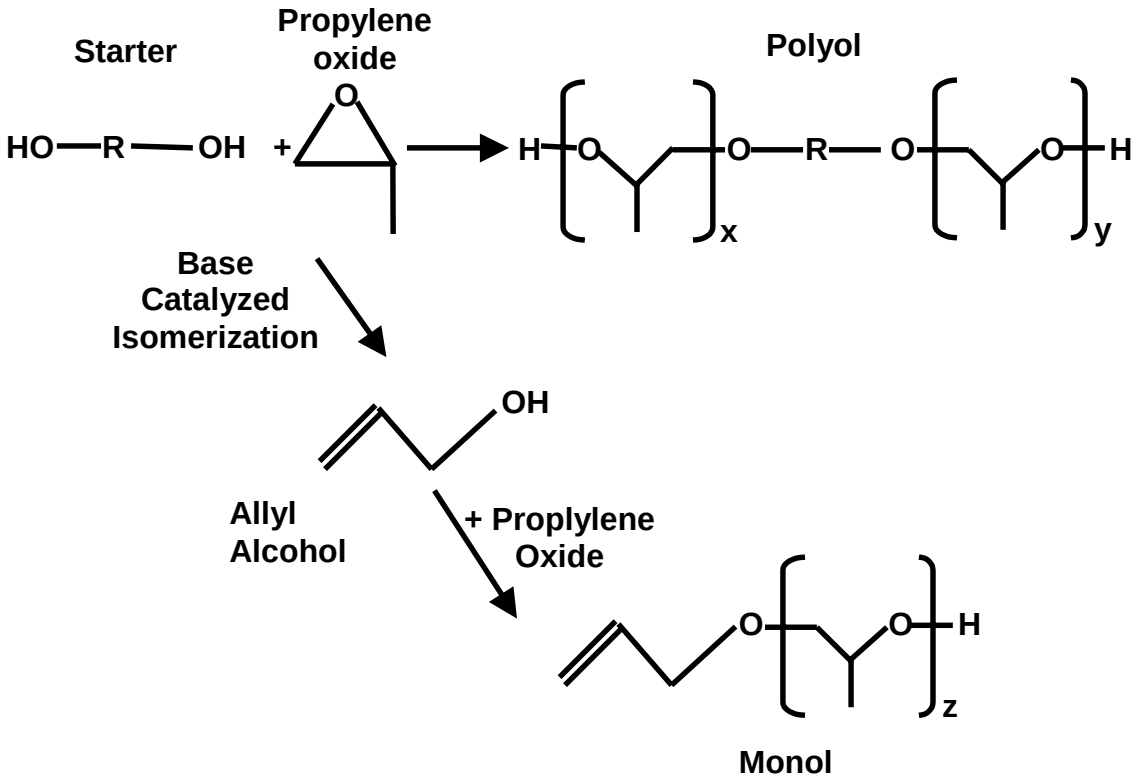

Figure 2-2. Base catalyzed production of poly(propylene glycol) primary product and monol side reaction product.[8]

poly(urethane-urea) chemistry is reviewed, acts as a chain terminator, limiting the

molecular weight of elastomers formed from it.[4] The level of monol may be determined through quantification of the amount of terminal double bonds.

Improvements to the production of polyols was achieved through General Tire's development and application of double metal cyanide catalysts (DMC).[5-7] These catalysts were less likely to promote the isomerization of propylene oxide into allyl alcohol, ultimately resulting in dramatically reduced monol content in the polyether polyol. A DMC catalyst developed by ARCO Chemical proved to be particularly effective in producing ultra-low monol content poly(propylene glycol)s. Figure 2-3 provides a comparison of the unsaturation level, which is indicative of monol content, for all three varieties of PPG, conventional, low monol, and ultra-low monol.[8] It is clear that substantial improvements in lowering monol content

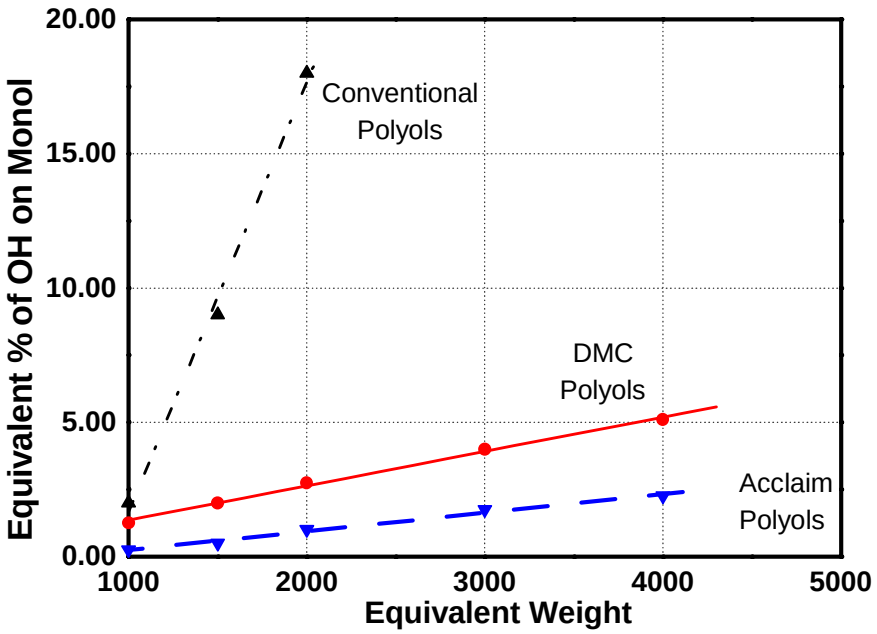

Figure 2-3. Monol content as a function of equivalent molecular weight for conventional base catalyzed PPG, DMC catalyzed PPG, and improved DMC catalyzed Acclaim PPG.[8]

have been achieved with both the DMC and ARCO catalysts. An explanation as to why the conventional polyol data did not extend beyond a molecular weight of 2000 g/mol will be provided shortly.

An essential aspect of synthesizing poly(urethane)s and poly(urethane-urea)s is knowledge of the chemical components' functionalities. In monol containing systems, the actual functionality may be calculated from Equation 2-1, which employs the measured unsaturation level mentioned above.[9] If then the

$$f = \frac{\left(\frac{OH}{56.1}\right)}{\left\{\left(\frac{OH}{56.1}\right) - unsat\right\}\left(\frac{1}{f_n}\right) + unsat} \qquad (2\text{-}1)$$

where,
f is the functionality,
OH is the hydroxyl number, mg KOH / g,
unsat is the unsaturation, meq / g,
f_n is the nominal functionality.

data shown in Figure 2-3 where used in conjunction with Equation 2-1, it would be seen that the actual functionality of the conventional poly(propylene glycol)s drops off rapidly with increasing molecular weight (Figure 2-4). When the functionality drops below ca. 1.7 it is often difficult to obtain a quality solid elastomer, particularly one with strong performance characteristics, when reacted with diisocyanates and chain extenders.[8] As was previously seen, as the molecular weight of the polyol increases, the amount of unsaturation or monol increases. For conventional base-catalyzed poly(propylene glycols) it was seen that a molecular weight of ca. 2000 g/mol corresponds to a functionality of 1.7 at which point the polyol proves unusable in elastomer production.

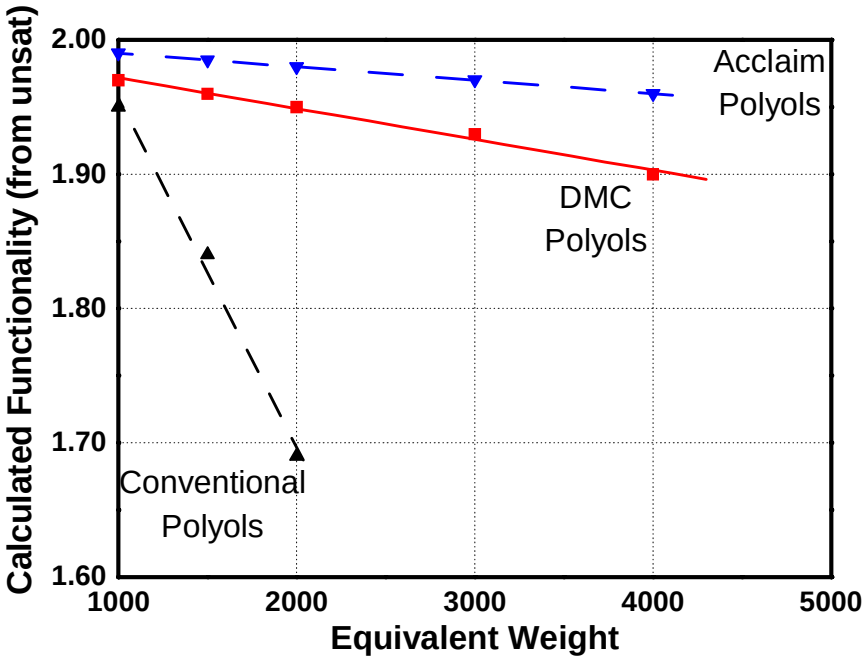

Figure 2-4. Calculated functionality as a function of equivalent molecular weight for conventional base catalyzed PPG, di-metal cyanide catalyzed PPG, and improved di-metal cyanide catalyzed Acclaim PPG.[8]

It has been seen that the poly(propylene glycol)s produced by Bayer will have significantly higher functionality in general and in particular, at higher molecular weights than those produced in the past by the conventional base-catalyzed process. Much of the literature regarding the use of PPGs in elastomers have focused on polyols with molecular weights 3000 g/mol or less, whereas in the present work, the PPG molecular weights range from 2000 g/mol up to 8000 g/mol.[8-15] The increased functionality of the polyols not only allows for increased polyol molecular weight and soft segment lengths, but will also allow for fabrication of much higher molecular weight elastomers. Employing the Carothers equation for theoretical molecular weight determination (Equation 2-2) to obtain the theoretical elastomer weight, it is seen that there exists an order of

$$\overline{x_n} = \frac{1}{1-p} \qquad (2\text{-}2)$$

where,

$\overline{x_n}$ is the average number of monomer residues per molecule,

p is the fraction of reacted groups present.

magnitude increase in molecular weight from those produced with the conventional polyols to those produced with the Bayer polyols (Figure 2-5).[16]

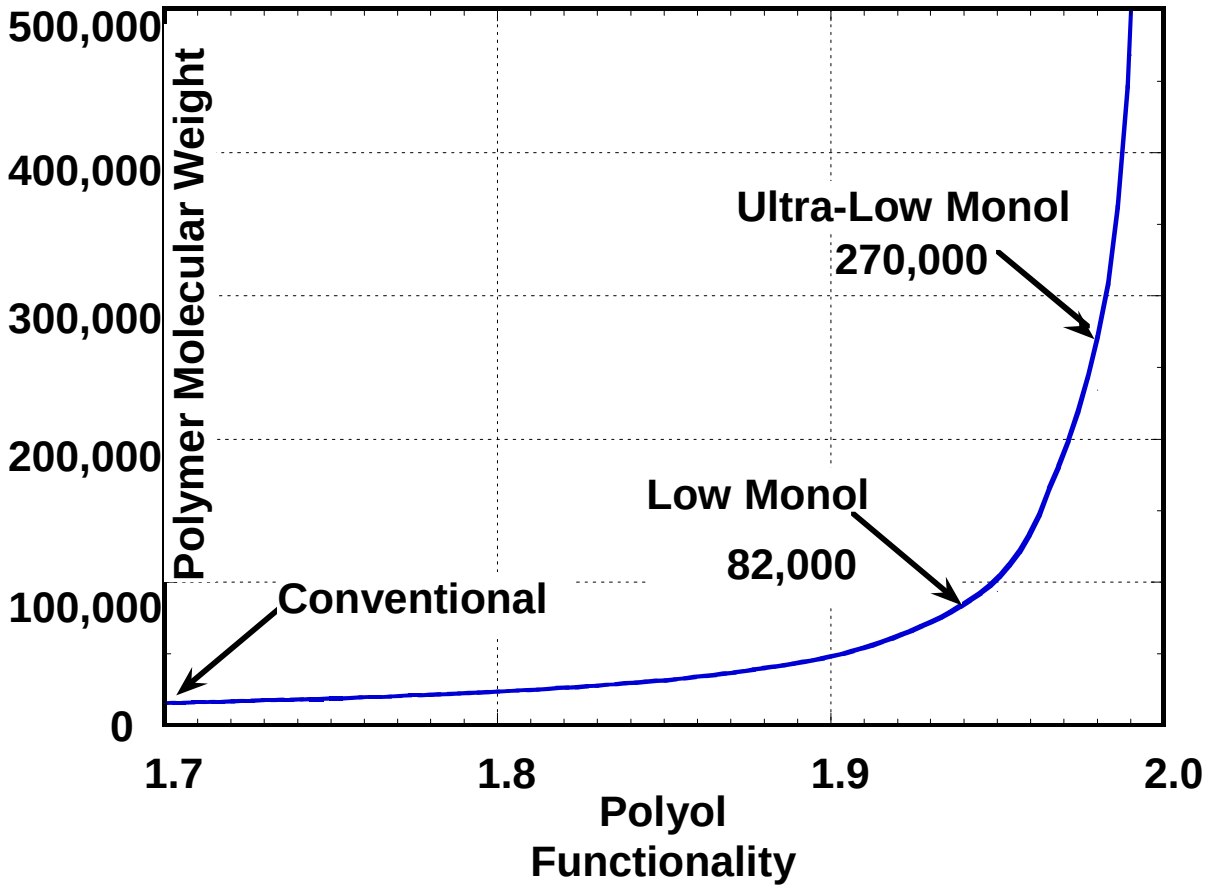

Figure 2-5. Theoretical elastomer molecular weight for 2000 g/mol PPG chain extended with BDO and MDI.[8]

Another aspect of the ultra-low monol polyols is that their molecular weight distribution is considerably narrower than conventional polyols (Figures 2-6 and 2-7). The narrower molecular weight distribution results in lower solution

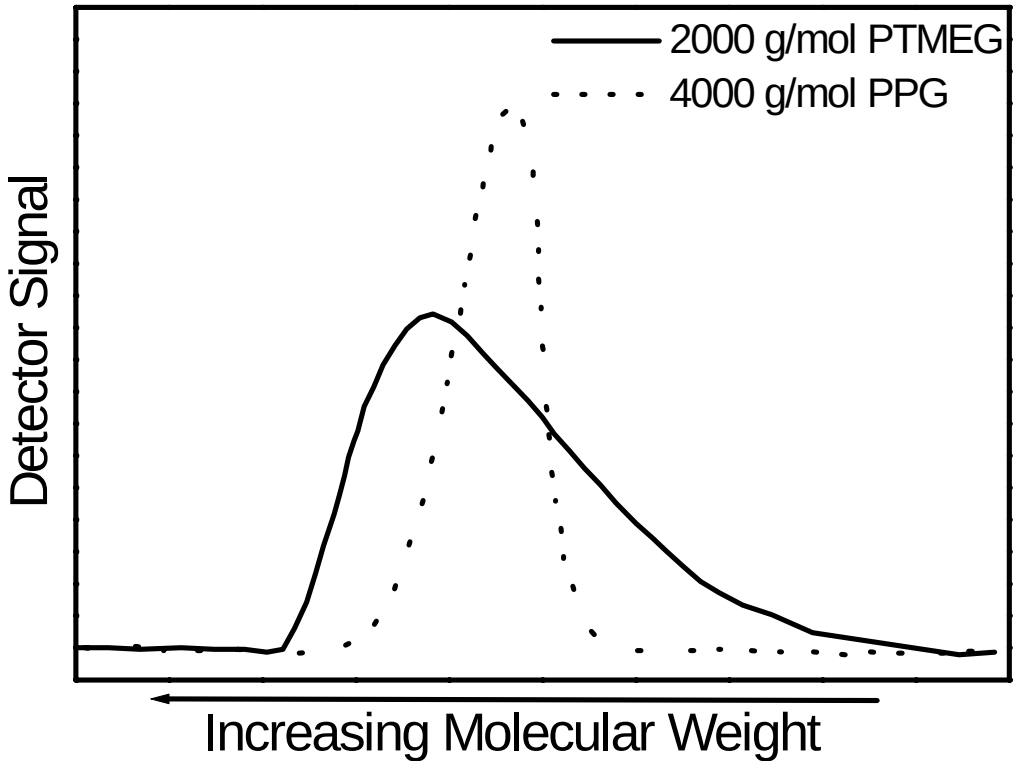

Figure 2-6. Comparison of molecular weight distributions of poly(tetra methylene ether glycol) and Acclaim PPG.[8]

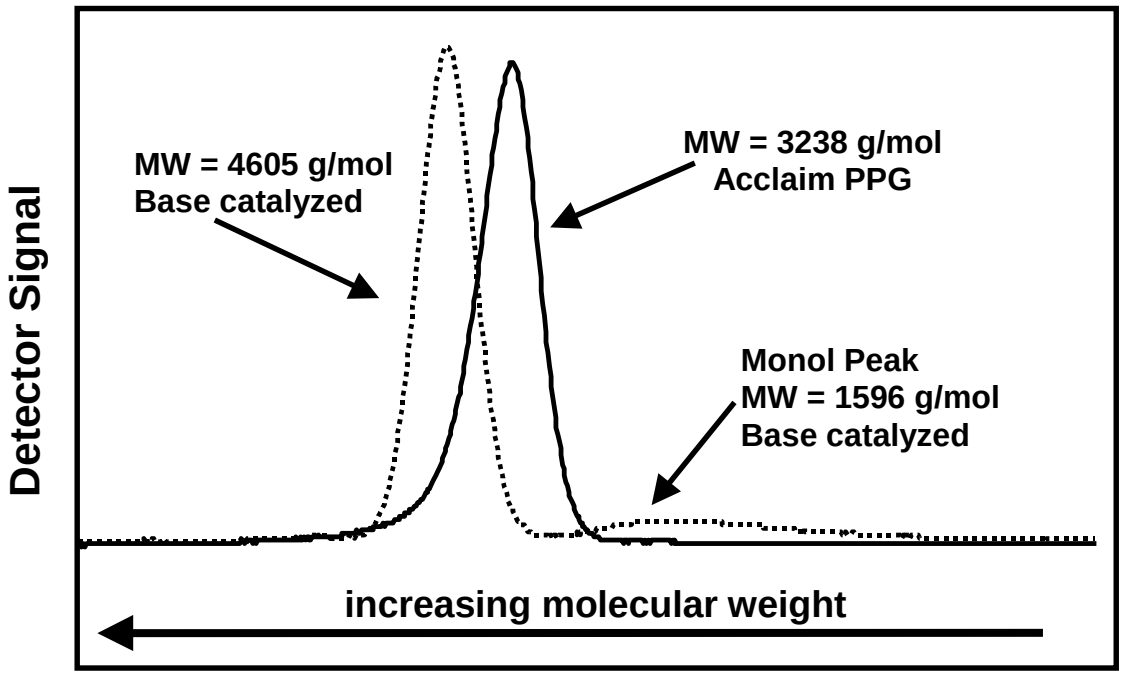

Figure 2-7. Comparison of MWD of conventional based catalyzed PPG (dotted line) and ultra-low monol content PPG with comparable number average molecular weights (provided by Dr. Bruce Lawrey of Bayer).

viscosities, in comparison to PTMEG based elastomers, which may be

advantageous with regards to processing of elastomeric fibers. Within the dry-spinning process commonly used for production of spandex fibers (Figure 2-8), the polymer solution is extruded from the spinneret into a hot chamber where the solvent is rapidly evaporated. Lower viscosities would allow for additional solids loading in the solutions, which results in a reduction of solvent amounts and/or greater throughput. Both possibilities would be enhancements to process

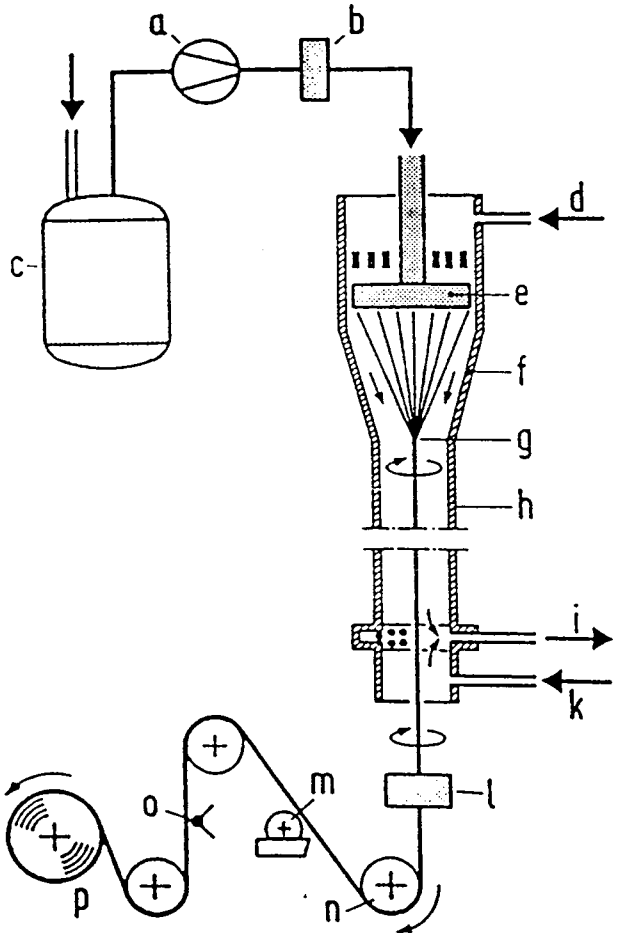

Figure 2-8. Dry Spinning Process Schematic. a) metering pump, b) filter, c) spinning solution, d) heated gas, e) spinnerets, f) heated spinning chamber, g) onset of twisting, h) chamber length ca. 4 to 8 m, i) hot gas exhaust, k) fresh gas, l) false twisting device, m) finishing (Schematic is a modification of a figure provided by Dr. Bruce Lawrey of Bayer).

economics and reduction of solvent amounts could have beneficial environmental ramifications.

Investigations into the potential of these new polyols in elastomeric applications have yielded promising results. When poly(urethane) elastomers made from conventional and Bayer 2000 g/mol and 4000 g/mol PPG were compared, the tensile strength and tear strengths were found to be improved and the de-mold time was found to be shorter (Table 2-1) for those based on Bayer PPG.[8] In the studies addressed by this document all materials will be poly(urethane-urea)s.

Table 2-1. Comparison of properties of polyurethane elastomers fabricated from ultra-low monol content PPG (Acclaim) and conventional PPG (Arcol). Data presented by Arco Chemical (now Bayer) at Fall 1995 Meeting of Poly(urethane) Manufacturers Association.[8]

	Acclaim PPG	Arcol PPG
molecular weight (g/mol)	2000	2000
monol content (meq / g)	.005	.022
polyol functionality	1.99	1.96
prepolymer composition		
% NCO prepolymer	4.0	4.0
NCO / OH	2.2	2.2
MDI (pbw)	27.7	27.7
2000 MW polyol (pbw)	100	100
prepolymer viscosity (cps)		
20°C	25000	22000
40°C	4600	4500
60°C	1450	1340
80°C	740	580
processing characteristics		
prepolymer (pbw)	100	100
1,4 butanediol (pbw)	4.2	4.2
potlife (minutes)	1-3	1-3
demold time (minutes)	20-45	30-60
elastomer properties		
hardness, Shore A	57	45 (39)
pendulum rebound %	60	58
ultimate elongation %	810	950
tensile strength (psi)	2300	919
100% modulus (psi)	200	134
200% modulus (psi)	260	163
300% modulus (psi)	360	209
400% modulus (psi)	510	274
die C tear strength (pli)	150	133
compression set %	29	56
compression deflection (psi)		
5%	40	n.d.
10%	80	n.d.
15%	120	n.d.
25%	222	n.d.

Section 2-2: Materials - Poly(urethane)s and poly(urethane-urea)s

Much of the credit for the development of poly(urethane) and poly(urethane-urea) chemistry is due to O. Bayer. The poly(urethane-urea)s used in this study are prepared by a two-step procedure, or prepolymer method as compared to a "one-shot" method. In the first step of the procedure (Figure 2-9), the polyols are reacted with a diisocyanate in excess to create isocyanate end-capped prepolymers. These end-capped prepolymers will become the soft

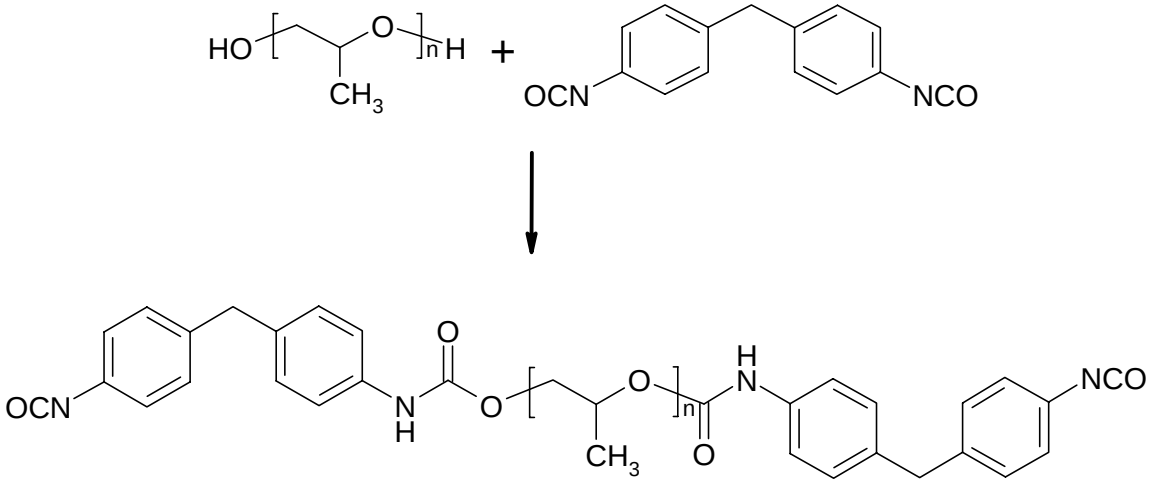

Figure 2-9. Synthesis of isocyanate end-capped PPG-based prepolymer.

segments of the poly(urethane-urea) and possess urethane linkages which will ultimately reside at the interface between hard and soft segments. It is possible that some polyols will be joined together by the diisocyanate, but largely they will exist as single end-capped polyols. The prepolymer will then be reacted with more diisocyanate and a chain extender (Figure 2-10). The choice of chain extender will determine whether the material is going to be a poly(urethane) or a poly(urethane-urea). If the chain extender is a diol, it will be a poly(urethane) and if it is a diamine, it will be a poly(urethane-urea). Throughout this study, the only

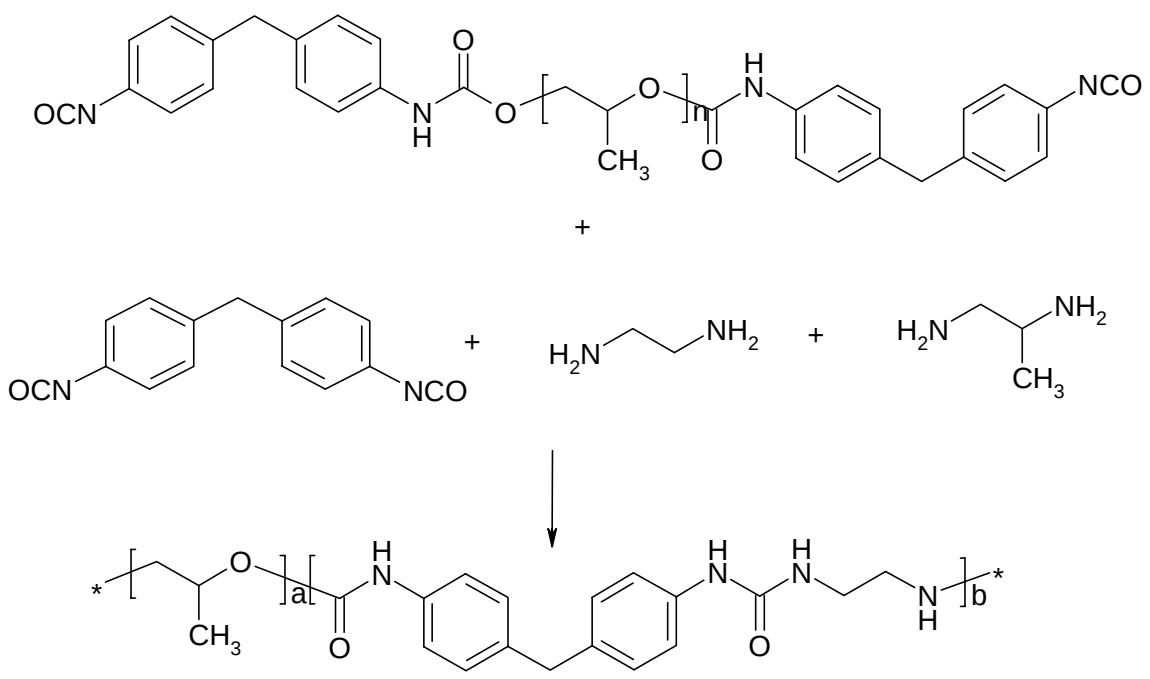

Figure 2-10. Chain extension of isocyanate end-capped PPG-based prepolymer with MDI and 80% EDA – 20% PDA diamine mix. Final structure shown with only EDA chain extender.

diisocyanate that will used is diphenyl methane diisocyanate (MDI). A variety of polyols will be used in the preparation of prepolymers and two chain extenders will be used in the second step of the synthesis (Figure 2-10), the properties of which are tabulated in Table 2-2. The two most predominantly used polyols within this study are poly(propylene glycol) and poly(tetramethylene ether glycol).

As mentioned above, PPG and PTMEG are the two polyols being investigated and it will facilitate the discussion to address a few key differences between the two polyols at this time (Figure 2-11). First, the PPG being investigated may be considered completely atactic, and is therefore unable to crystallize. PTMEG on the other hand, may undergo strain-induced crystallization as well as crystallization below room temperature when used in PU

Table 2-2. Properties of component reagents (data from Aldrich Chemical Catalog and Dr. Bruce Lawrey of Bayer).

component	FW (g/mol)	T_g (°C)	T_m(°C)	ρ (g/cm^3)
N,N dimethylacetamide (DMAc)	87.12		-20	0.937
PTMEG 2000	2000		28-40	0.972
PPG 1000	1000	-70.41	n/a	1.004
PPG 2000	2000	-69.12	n/a	1.004
PPG 4000	4000	-67.97	n/a	1.004
PPG 8000	8000	-67.82	n/a	1.004
PPG 12000	12000	-67.82	n/a	1.004
4, 4' Methylenebis (phenyl isocyanate) MDI	250.26		42-44	1.180
1,2 propylene diamine (PDA)	74.13		n/a	0.870
1,2 ethylene diamine (EDA)	60.10		8.5	0.899

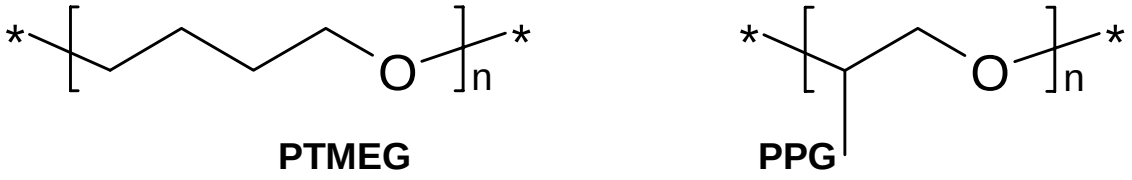

PTMEG **PPG**

Figure 2-11. Poly(tetra methylene ether glycol) and poly(propylene glycol).

and PUU elastomers. This assumes sufficient molecular weight of the PTMEG (~2000 g/mol and higher) and phase separation of the elastomer. PTMEG of 2000 g/mol molecular weight is a waxy solid at room temperature and melts between 30-40C. The melting temperature of PTMEG, both by itself and when used in elastomers, increases with molecular weight. The potential presence of crystallinity can have a significant effect upon the material properties. Second, the mass per backbone bond differs between the polyols (Table 2-3). PPG has a pendant methyl group and only a pair of backbone carbons, while PTMEG has four backbone carbons. On a basis of a 2000 g/mol average polyol, there will be 139 backbone bonds in PTMEG, while there will only be 103 backbone bonds in

Table 2-3. Comparison of PPG and PTMEG.

Polyol	MW per repeat unit (g / mol)	Backbone bonds per repeat unit	Mass per Backbone Bond (g / mol)	MW Between Entanglements (g / mol)[75]
PTMEG	72	5	14.4	2500
PPG	58	3	19.3	7700

PPG. Table 2-3 and Figure 2-12 illustrate these differences in molecular weight per backbone bond and as a function of polyol molecular weight. Third, PPG has a pendant methyl group that results in a greater chain cross-sectional area than PTMEG. This results in fewer PPG chains that can cross a unit cross-sectional area relative to PTMEG segments. Fourth, the molecular weight necessary for

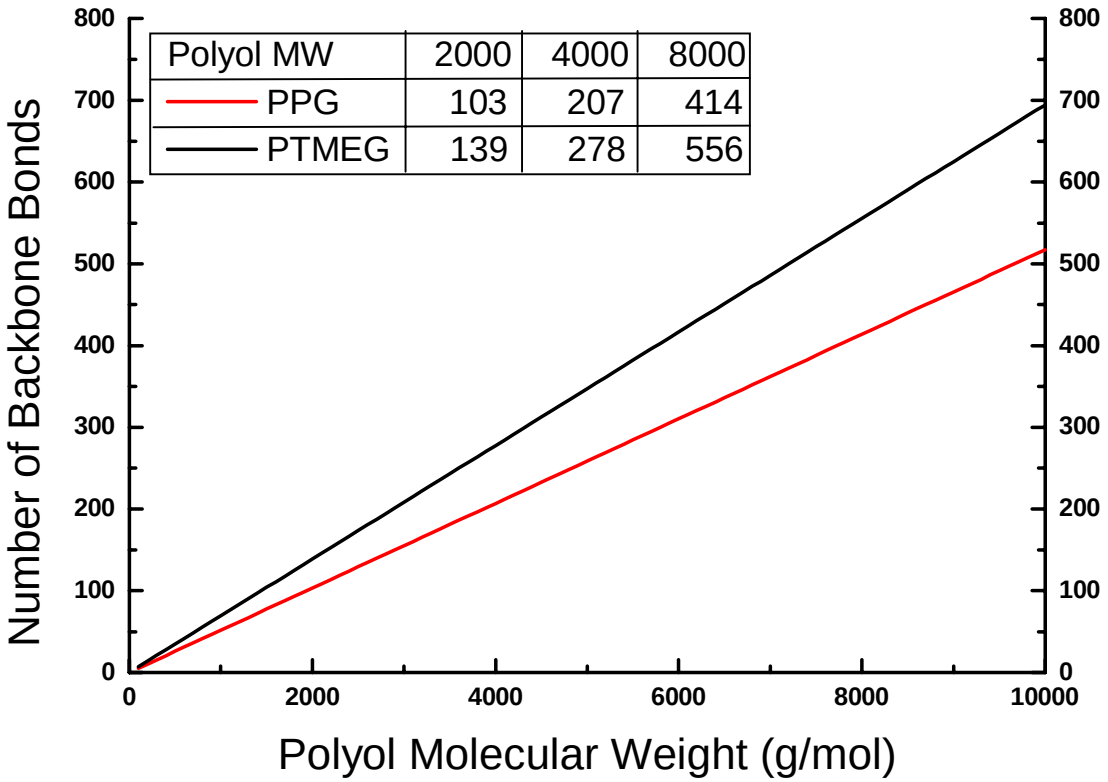

Figure 2-12. Number of polyol backbone bonds as a function of polyol for PPG and PTMEG.

entanglements, MW_e, differs greatly for the two polyols, PPG having the higher value of 7700 g/mol (Table 2-3). Fifth, the two polyols differ in their optical anisotropy, due largely to the pendant methyl group in PPG. The polarizabilities down the chain axis and perpendicular to it will differ. Hence an optical anisotropy is inherent in each repeat unit type and these optical anisotropies will differ from one another, with that of PTMEG being the higher. Finally, ultra-low monol content PPG has a much narrower molecular weight distribution than most commercially produced PTMEG (Figure 2-6). Little work has been done to narrow the molecular weight distribution of PTMEG.[18-20] Most studies involving narrow MW distribution PTMEG entail the fractionating of a broader MW distribution PTMEG.[21]

Often, the chain extender is a blended mixture of diamines in an attempt to disrupt the symmetry of the hard segments. It has been found that when only ethylene diamine (EDA) was used, there existed a greater possibility that the hard segments would hydrogen bond too strongly forming “physical” gels within the spinning solutions.[17] These gels prove to be deleterious to the spinning process and are to be avoided. Propylene diamine (PDA) is often used in conjunction or in lieu of EDA in order to alleviate potential gelation problems.[17]

Section 2-3: Materials - Microphase Separation

Microphase separation can occur in block copolymers when the blocks consist of two chemically incompatible segments. If the system were a blend of incompatible homopolymers instead of covalently linked polymer blocks and the molecular weights of the polymers were sufficiently high, the two components will attempt to separate into two distinct macrophases with isolated instances of chain mixing. However, since the blocks are covalently linked, they are restricted with regards to the scale length over which they may separate. Considerable work has been done in attempt to explain and predict how, when, and to what extent separation will occur.[22-25] Many of the explanations ultimately rest in the realm of thermodynamics, and in particular with arguments based upon issues of solubility. The miscibility behavior of mixtures of low molecular weight materials may be characterized by the solubility parameter, δ, of each component, where a general rule of thumb is that miscibility occurs when $\delta_1 \approx \delta_2$.[26,27] This approach is limited when applied to polymers with high levels of secondary bonding, and it is often more advantageous to implement Hansen's concept of a three-dimensional solubility parameter which includes contributions of hydrogen bonding, permanent dipole interactions, and dispersion forces.[26] The quantity within the parentheses is often termed the cohesive energy density and there exist obvious difficulties in directly obtaining values of it in the case of polymers.[28-30] However, indirect methods for measuring ΔE_v do exist, and there are number of methods by which the solubility parameter δ itself can be estimated.[31-34] Often the quantity of interest in predicting whether two polymers or blocks will phase separate is the

differential solubility parameter Δ_{12} which is defined in Equation 2-3.[35] Molecular

$$\Delta_{12} = \delta_1 - \delta_2 \qquad (2\text{-}3)$$

where,
Δ_{12} is the differential solubility parameter,
δ_i is the solubility parameter of the ith component.

weight of the blocks will influence separation characteristics. For example, when the molecular weight of the two components is low, Δ_{12} must be large for separation to occur.[36] As in any thermodynamic explanation, the effect of temperature is also an important consideration when pondering whether two polymers or blocks will phase separate.

As mentioned above, two or more chemically incompatible blocks must be linked covalently. When the use temperature is in excess of the glass transition of one of the blocks, that block is said to be the soft block or soft segment. A phase formed of soft blocks or segments, is referred to as being the soft phase or domain. A block or segment that exists below its glass transition or in some cases its crystallization temperature is referred to as the hard, or occasionally glassy, block or segment. Similarly, regions rich in hard blocks or segments are referred to as hard domains or phases. This is schematically represented in simplistic form (Figure 2-13) where the soft phase is in majority. The volume fractions of the two phases, ϕ_S and ϕ_H, are a large factor in determining whether the material will behave as a toughened solid or as an elastomer. When the hard phase is in majority or continuous, the soft domains will act as toughers and in this way such block copolymers resemble conventional toughened thermoplastics (Figure 2-14). On the other hand, when the soft phase is in

majority, the hard domains will play the role of physical crosslinks or tie-points. These physical crosslinks or tie-points will mimic covalent crosslinks in their role of developing a polymer network creating in effect elastomeric materials. The hard domains also act as reinforcers in the elastomer. This proposed study concentrates exclusively upon the case where the soft phase is in the majority and elastomeric materials are obtained. When the soft phase is the continuous phase, there will exist an average distance between the minority hard domains, and possibly also an average domain size. In general, the regions rich in soft segments will be referred to as the soft phase and the regions rich in hard segments will be referred to as the hard domains.

The phenomenon of microphase separation has been studied in great detail for a variety of elastomeric materials.[22-25, 37-41] Much of the well known work was done on the earliest synthetic rubbers and materials such as Kraton which is a triblock copolymer.[42-43] While these materials are block copolymers, they differ in a number of ways from the poly(urethane)s and poly(urethane-urea)s which are the focus of this study.[44] First, the molecular weights of the blocks in copolymers such as Kraton are much higher than those of the poly(urethane-urea)s. Second, for equal molecular weight elastomers, there are far fewer individual segments or blocks per polymer chain in the Kraton materials than in the segmented block copolymers such as poly(urethane)s and poly(urethane-urea)s. Third, the distribution of block sizes is broader for most PU and PUU commercially produced elastomers than for Kraton materials. Also, there exist thermodynamic considerations, such as solubility, dependent upon

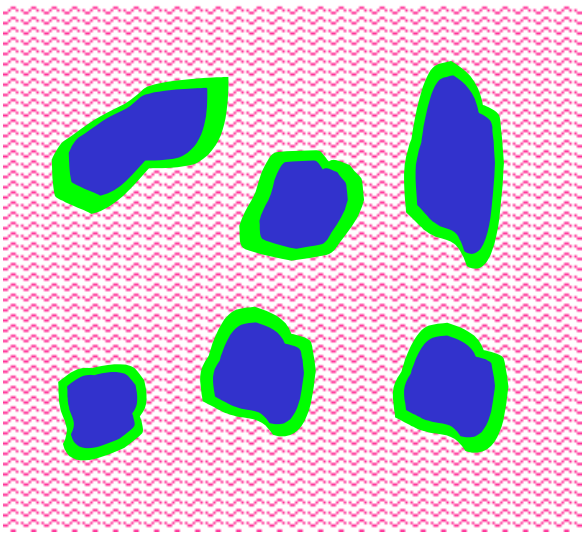

Figure 2-13. Simplistic schematic of a microphase separated material where pink indicates the major phase (soft phase), blue the minor phase (hard domains), and light green the interphase region between the phases.

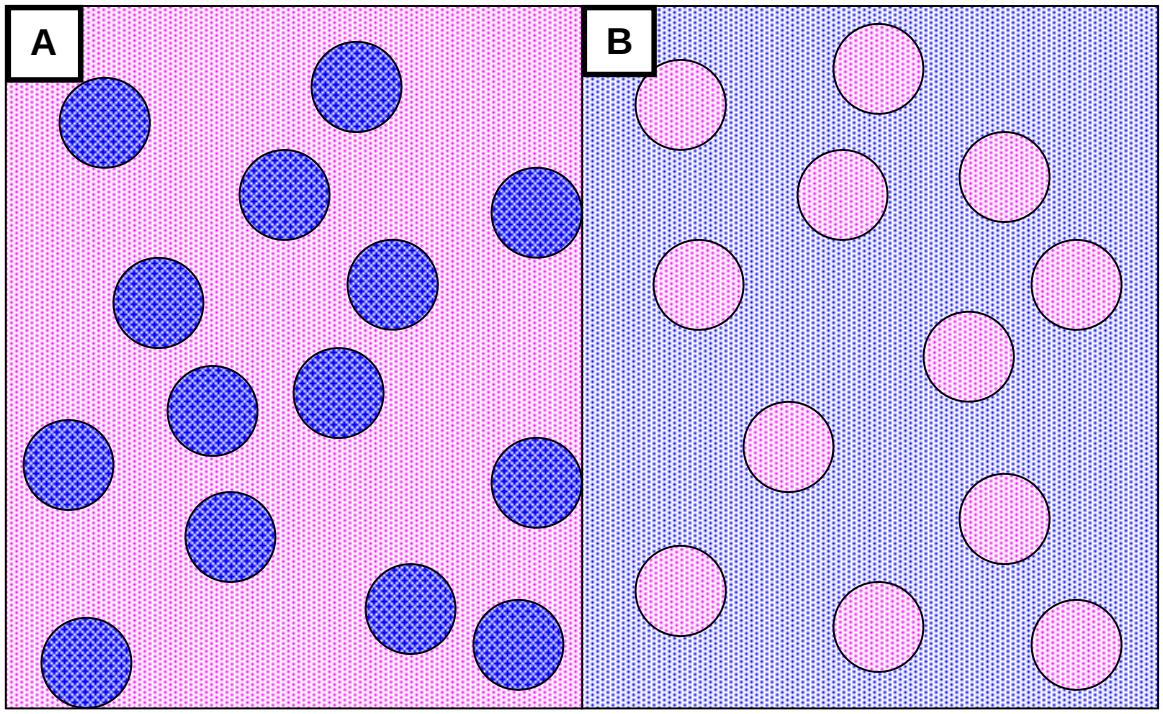

Figure 2-14. Reinforced elastomer (a) and toughened plastic (b), where blue indicates hard or glassy material and pink indicates soft or rubbery material.

the molecular weights of the blocks. These aspects result in decreased distances between domains, which are generally smaller, and less complete

phase separation. Fourth, the poly(urethane)s and poly(urethane-urea)s contain backbone heteroatoms, such as oxygen and nitrogen, that instill considerable polar character to some of the segments and allow for considerable hydrogen bonding in a number of cases.[44] In fact, in the case of many poly(urethane-urea)s, the hydrogen bonding is substantial enough that the thermal degradation occurs before effective melt processing can be achieved. In contrast, the Kraton materials can be melt-processed and denoted as thermoplastic elastomers for this reason. Further discussion regarding secondary bonding in the poly(urethane)s and poly(urethane-urea)s will be forthcoming.

Though the two segments, hard and soft, are not completely chemically compatible, complete phase separation, as in the case of two incompatible homopolymers, rarely occurs. Three sources contribute to the incompleteness of phase separation. First, individual hard segments may be solubilized in the soft phase, adding some restriction to soft segment mobility. Second, conversely, individual soft segments may be present within the hard domains. These first two scenarios will be most often described in terms of phase mixing. And third, there may exist an interphase between the soft phase and hard domains where both segments are required to co-exist (Figure 2-13). Choice of the descriptor interphase, rather than interface, to describe the region between the hard domains and soft phase was deliberate and reflects the philosophy of Professor J. P. Wightman. Wightman argues that an interface is by definition one dimensional (a plane), and what is most often being described is in reality a three dimensional region (a volume).[45] The degree or extent of phase separation will

often effect the thermal and mechanical properties and will need to quantified both in terms of phase mixing and size of the interphase.[23-24, 46-47] Recent studies by Garret et. al. have proposed that the extent of phase mixing in some

Table 2-4. Experimental techniques applied in this study.

Structural Aspect	Experimental Technique	Information Obtained
microphase separation	SAXS AFM DMA DSC	interdomain spacings interphase thickness phase mixing surface micrograph
crystallization	WAXS DMA DSC	strain-induced crystallization cold crystallization relative potential for crystallization
dynamic mechanical	DMA	E'(T) and E''(T) Damping Characteristics T_m, T_g, T_β
thermal	DSC	T_m, T_g, ΔC_P, ΔH_f
molecular orientation	birefringence	birefringence which scales with the system average chain orientation
segmental orientation	infrared linear dichroism	segmental orientation function
thermal degradation	TGA	mass loss as a function of temperature mass loss as a function of time

poly(urethane-urea)s has been greatly underestimated.[47] This is contrary to the findings of many earlier studies which imply that PUUs exhibit good phase separation.[15,23-24,37-38,40-41,46]

Hints and insights into the microphase separation characteristics, domain size, domain spacing, phase mixing, and interphase thickness, may be obtained through a myriad of microscopy, thermal, and mechanical analytical techniques. A brief accounting of those techniques used within this study are presented here and summarized in Table 2-4. More in depth discussion of the individual methods is provided in the experimental methods review. Information regarding

interdomain spacing for the entire polymer sample is best obtained from small angle x-ray scattering (SAXS). Small angle x-ray scattering may also provide a quantitative measure of the interphase thickness, σ, and other morphological parameters. Atomic force microscopy (AFM) may be used to examine the polymer surfaces and confirm features and trends seen with small angle x-ray scattering. It can also yield, in some cases stunning, micrographs of microphase separation on the surface, which presumably reflect the behavior of the bulk material, of polymer samples. Dynamic mechanical analysis (DMA) and differential scanning calorimetry (DSC) provide methods for probing the microphase separation characteristics through changes in the glass transitions of the components. In practice in poly(urethane-urea)s the soft segment glass transition is of much greater utility for this type of investigation since the hard segments are often hydrogen bonded to the extent that the material will thermally degrade before softening substantially or before any MDI-Diamine crystals will melt. It was suspected a priori, from knowledge of the polymer synthesis procedure, that the materials in this study should be block copolymers that should undergo microphase separation. This was verified with by using the methods described above.

Section 2-4: Materials - Hydrogen Bonding

It has already been mentioned that within poly(urethane)s and poly(urethane-urea)s there exists potential for hydrogen bonding or varying magnitude. Examination of a typical poly(urethane) (Figure 2-15) reveals that there exists a potential of hydrogen bonding between the hydrogen of a urethane group (proton donor) and either the oxygen of a urethane carbonyl or the oxygen

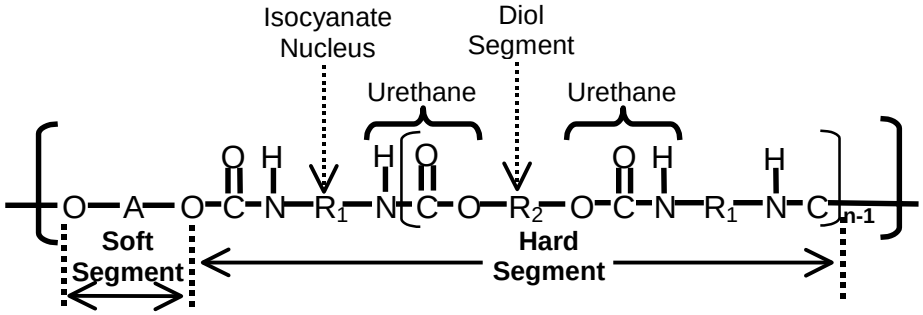

Figure 2-15. Structure of generalized poly(urethane).[27]

of an ether group (proton acceptors). Schematics (Figure 2-16a and 2-16b) of various hydrogen bonding possibilities is presented by Painter et al.[48-49] Hydrogen bonding of the urethane carbonyl groups has been well characterized by Fourier transform infrared spectroscopy studies by many researchers where it has been seen that hydrogen bonding results in a shift in the absorption of the urethane carbonyl to lower wave numbers (Figure 2-17, Table 2-5.).[48-60] It has been seen that the strength and degree of hydrogen bonding in poly(urethane)s decreases with temperature.[60]

Poly(urethane-urea)s undergo hydrogen bonding in a similar fashion with one very significant difference which will be discussed shortly. Again, perusal of a representative poly(urethane-urea) (Figures 2-18 to Figure 2-20) reveals the potential for hydrogen bonding. In this instance there are two possible proton donors, the hydrogen of the urethane linkage and the hydrogens of the urea

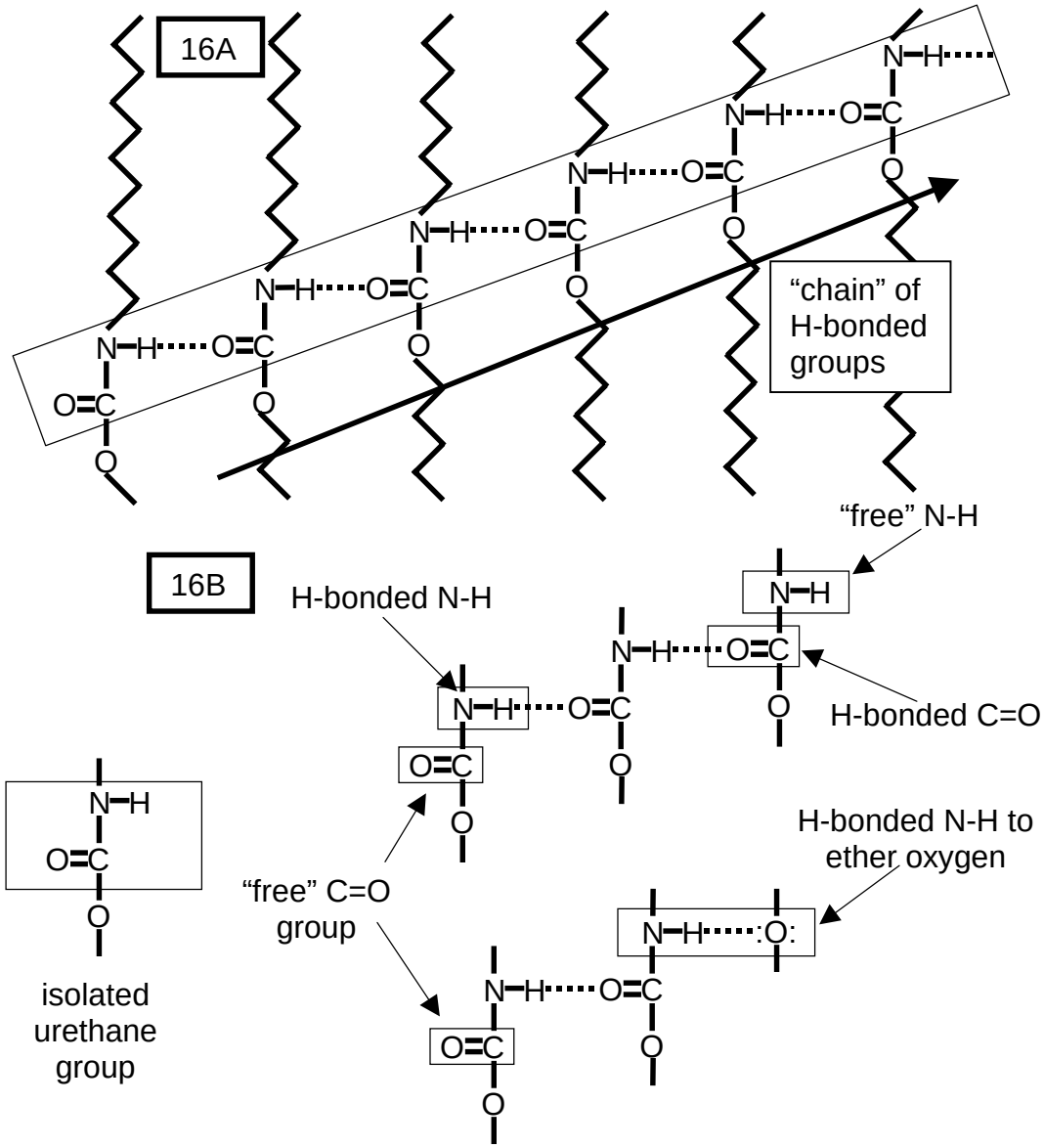

Figure 2-16. Hydrogen bonding in poly(urethane)s. 16A – "chains" of hydrogen bonds, 16B various hydrogen bond interactions. [1-2]

linkage, and three possible proton acceptors, the ether oxygen, the urethane carbonyl oxygen, and the urea carbonyl oxygen. The key difference is that each of the two hydrogens in a urea linkage may form hydrogen bonds to a single carbonyl oxygen as shown by Sheng-Kang for some model poly(urethane-urea)s (Figure 2-19).[60] This hydrogen bonding scenario is dubbed bidentate, for it

Table 2-5. FTIR band assignments for poly(urethane-urea)s, exclusively hard segment absorptions in blue, predominantly soft segment absorptions in pink.[1-14]

wave number (cm^{-1})	assignment
3480	ν(NH) free
3289, 3270	ν(NH) h-bonded
2980	$\nu(CH_3)$
2860	$\nu(CH_2)$
2270	ν(NCO)
1729-39	ν(C=O) free urethane carbonyl
1706-1713	ν(C=O) h-bonded urethane carbonyl
1691	ν(C=O) free urea carbonyl
1666 (1659-1678)	ν(C=O) h-bonded disordered urea carbonyl
1628-1643	ν(C=O) h-bonded ordered urea carbonyl
1540	δ(N-H)+ν(C-N) amide II
1488, 1471, 1451, 1417	$\delta(CH_2)$
1240	δ(N-H)+ν(C-N) amide I
1110	ν(C-O-C) ether group

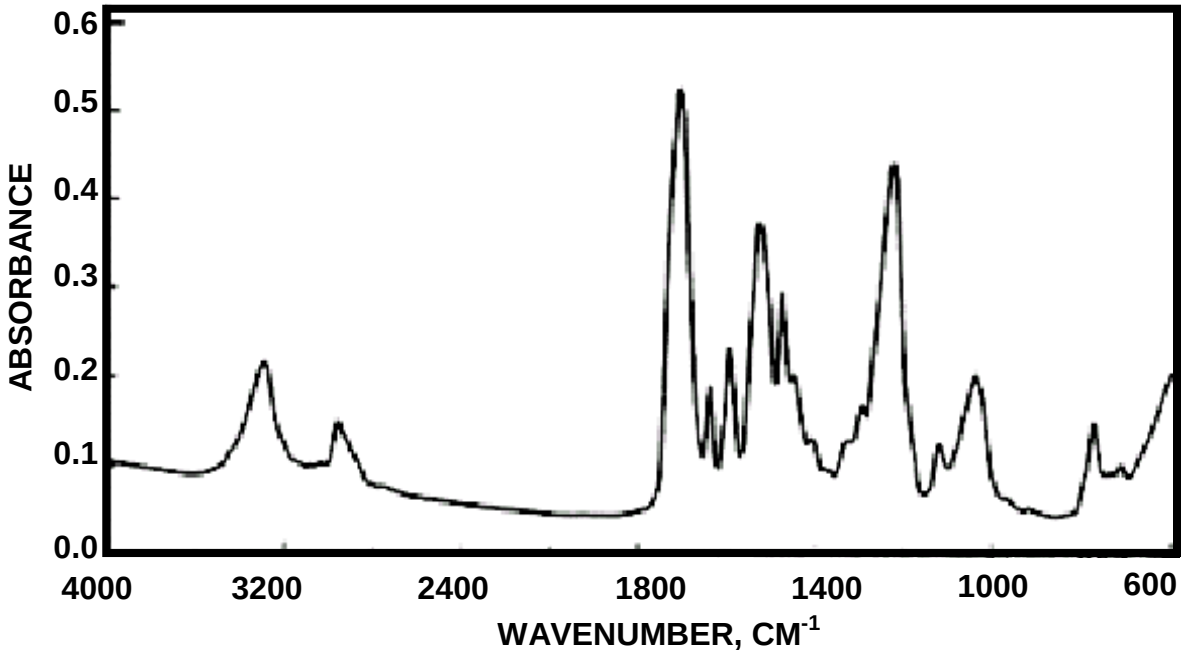

Figure 2-17. FTIR spectra of model hard segments of 2,4 TDI-BD.[56]

appears that two “teeth” are biting into a carbonyl oxygen. It was seen that there existed a shift in the urea carbonyl absorption band from ca. 1690 cm^{-1} for the

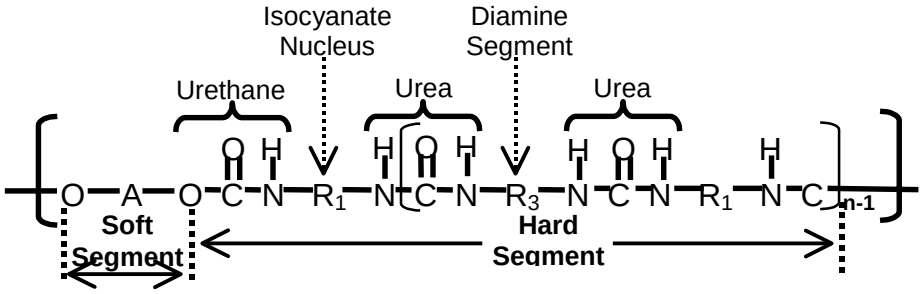

Figure 2-18. A generalized poly(urethane-urea).[26]

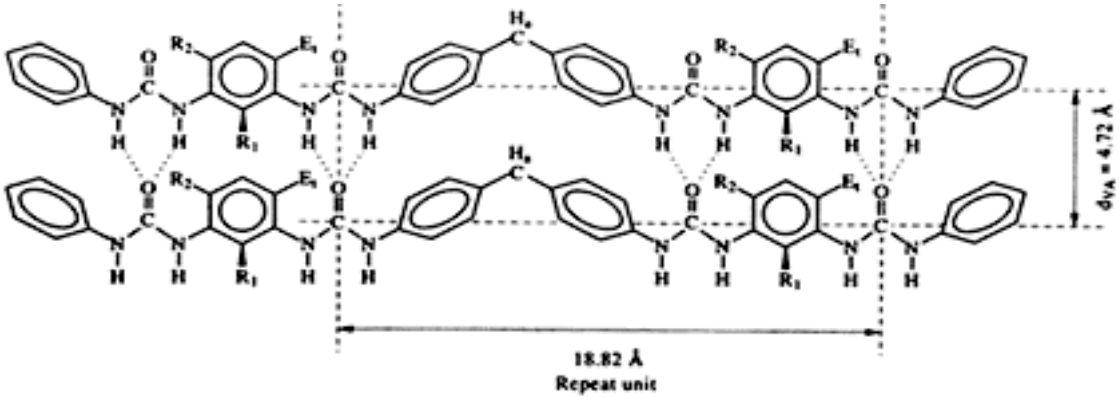

Figure 2-19. Model compound investigated by Sheng-Kang.[14]

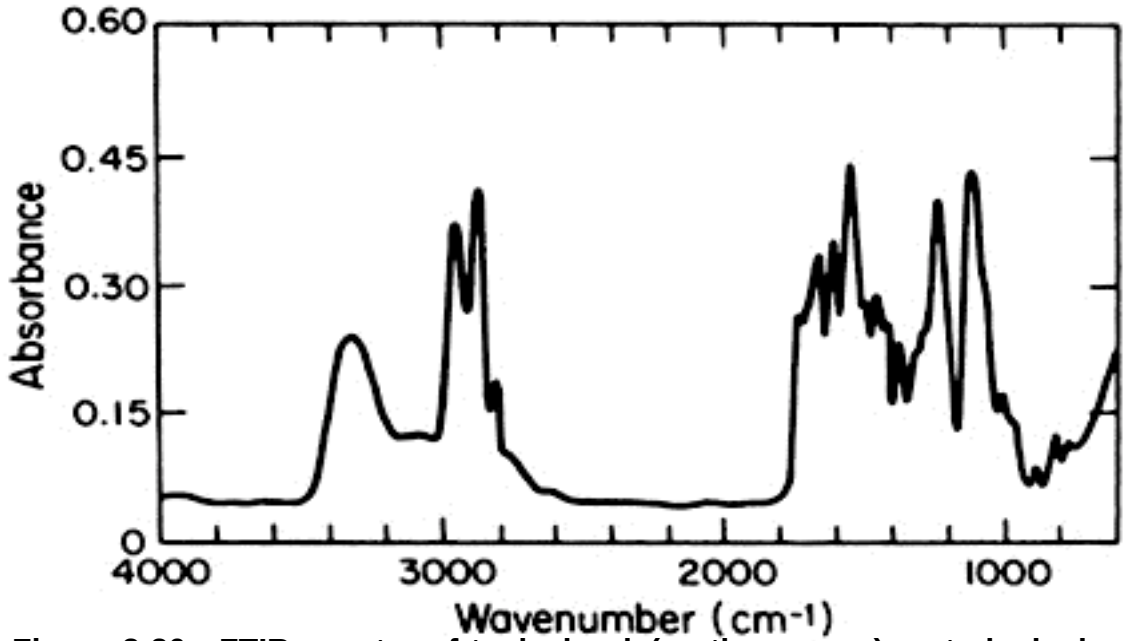

Figure 2-20. FTIR spectra of typical poly(urethane-urea), note inclusion of urea carbonyl absorptions between 1630-1700 cm^{-1}.[10]

non-hydrogen bonded case to ca. 1638 cm^{-1} for the hydrogen bonded case.[57,60]

Bidentate hydrogen bonding of poly(urethane-urea)s does not diminish with

temperature as it does with poly(urethane)s (Table 2-6), and it is often the case that the bidentate hydrogen bonding will persist up to the point where thermal degradation of the polymer has begun.[17] It was proposed by Sung and Bonart, and supported by Cooper that in poly (urethane)s and poly(urethane-urea)s there existed a "three dimensional hydrogen bonding" that has substantial impact on the mechanical properties of the elastomer.[53, 55, 61] For instance, in those cases where the hard segment chemical composition was chosen to minimize extensive hydrogen bonding, it was seen that in comparison to analogous poly(urethane)s, the poly(urethane-urea) materials had a substantially higher hard segment glass transition temperature.[53,56] It was also seen, that the soft segment glass transition was substantially less sensitive to changes in hard segment content in poly(urethane-urea)s than in poly(urethane)s.[53] Perhaps one of the most important consequence of the bidentate or three-dimensional hydrogen bonding in poly(urethane-urea)s, is that such systems, while having enhanced properties when compared to analogous poly(urethane)s, are not readily melt processed and must be spun from solution.[17]

Table 2-6. Hydrogen bonding as a function of temperature for poly(urethane)s and poly(urethane-urea)s.

T (°C)	poly(urethane) urethane linkages		poly(urethane-urea) urethane linkages		poly(urethane-urea) urea linkages	
	bonded	**free**	**bonded**	**free**	**bonded**	**free**
30	1.01843	1.83410	0.93454	1.94848	0.29488	**n.a.**
45	0.98618	1.85253	0.91413	1.97797	0.31529	**n.a.**
90	0.95161	1.90323	0.86196	2.03921	0.29488	**n.a.**
135	0.90092	1.97005	0.78030	2.12994	0.30395	**n.a.**
180	0.85023	2.02074	0.73040	2.20253	0.30395	**n.a.**
200	0.81567	2.03917	0.72132	2.21160	0.30395	**n.a.**

While it is not the intent of this study to reaffirm that hydrogen bonding, and particularly bidentate or three-dimensional, occurs in poly(urethane-urea)s it is of importance that it is appreciated why it is not yet possible to melt process spandex in an economical fashion while maintaining quality elastomeric properties. There exists a great wealth of information regarding the hydrogen bonding of poly(urethane) and poly(urethane-urea) elastomers, of especial interest is the work of Ishihara, Sung, Cooper, MacKnight, Coleman, Bonart, and Sheng-Kang.[50-64]

Section 2-5: Materials - Spandex

Spandex fibers were the result of a desire to improve upon "natural" rubber fibers and were first invented in the 1950s. Rubber fibers, whether produced by cutting rectangular cross-section fibers from rubber sheet, or from latex which is extruded into coagulating baths, are produced slowly in comparison to synthetic fiber spinning processes.[65] Additionally, rubber fibers were subject to degradation in ambient atmospheric conditions due to the presence of the double bond in cis-polyisoprene. As such, rubber fibers were deficient in terms of both process economics and material properties and there was a motivation to find satisfactory synthetic replacements.

Elastomeric materials developed as a nearly inevitable extension of work in the area of segmented polymers, particularly block copolymers where the blocks are chemically dissimilar. The development of poly(urethane) foams provided impetus for the investigation of a myriad of segmented block copolymers. It was shown by Wittbecker that elastomeric properties could be obtained from some copolyamides where one polyamide segment was high-melting and hydrogen bonded and the other polyamide segment was low-melting and non-hydrogen bonded.[66] Further studies by Snyder, Shivers, Edgar and Hill continued to develop the field, particularly with respect to the usage of various polyethers as “soft segment” material.[67-68] Two important aspects were developed during this time that proved quite pertinent to the eventual development of what is currently known as spandex. First, a set of criteria, presented in Table 9, were set forth by Shivers for the chemical requirements for synthetic elastomeric fibers and second it was recognized that polymerized

Table 2-7. Shivers' criteria for segmented polymers useful for elastomeric fibers applications.[17]

1	soft segments of low-melting polymers forming the major part of the segmented elastomers
2	hard segments consisting of blocks of high-melting polymers held together by hydrogen bonding or other forces
3	stability of hard and soft segments during the synthesis and processing of the segmented polymers
4	no covalent crosslinks required

tetrahydrofuran yielded poly(tetramethylene ether glycol) which was especially advantageous for use as a soft segment. Poly(tetramethylene ether glycol) or PTMEG is also known by a number of other monikers (summarized in Table 1-1.) such as poly(tetrahydrofuran) or PTHF and poly(tetramethylene oxide) or PTMO. It will, in this work, be most often referred to as poly(tetramethylene ether glycol) or PTMEG.

Given the initial criteria for elastomeric fibers presented in Table 9., there are obviously many chemical combinations usable to achieve elastomeric properties. Ultee provides a generalized description of some of these possibilities which have been summarized in Table 2-9.[17] Considerable recognition is due to O. Bayer (Figure 2-21) whose polyaddition process opened the way for production of polyurethanes.[69] It was at I.G. Farben, later Bayer, that the first polyurethane fibers were made and it was due to the efforts of

Table 2-8. Ultee's list of soft and hard segments useful for elastomeric fibers.[17]

soft segment choices	hard segment choices
polyethers	**poly(urethane)s**
polyesters	**poly(urea)s**
polylactones	**poly(amide)s**
	polyesters

Figure 2-21. Otto Bayer.[5]

researchers at Bayer and DuPont that eventually led to what are now recognized as spandex fibers.

DuPont introduced “Fiber K”, a dry-spun spandex fiber in 1959 based upon a PTMEG soft segment. Fiber K became known as Lycra™ in 1962 when it went from a pilot plant product to commercial plant production.[17] The fibers were dry spun (Figure 2-8) from a solution of the polymer in dimethyl formamide (DMF). Bayer was somewhat less motivated at this time to produce a fashion fiber due to the lingering aftereffects of the second world war in Germany and did not aggressively pursue commercialization during the 1950s. However, they quickly responded to developments in the United States in the late 1950s and introduced the first commercial version of “Dorlastan” in 1964.[70] Dorlastan was a dry-spun spandex fiber spun from solutions of polymer and dimethyl acetamide

(DMAc). The Bayer polymer used a polyester as a soft segment as compared to DuPont's polyether soft segments. Like DuPont, Japan's Toyobo also produced a dry-spun spandex, "ESPA", in 1962, theirs being based upon PTMEG soft segments and hard segments comprised of diphenyl methane diisocyanate (MDI) and 1,2 propylene diamine (PDA).[71]

Developments in the understanding of the structure-property relationships, particularly by Schollenberger, Tobolsky, Cooper, and Bonart, of poly(urethane-urea)s and spandex in particular led to the appreciation that attempts at covalent crosslinking of the chains was unnecessary and possibly even detrimental. The strong hydrogen bonding between hard segments leads to formation of regions rich in hard segment, the so-called hard segment domains.[46,72-73] These hard domains act as physical crosslinks which often lead to elastomer properties superior to those with covalent crosslinks. Schollenberger first described these physical or virtual crosslinks in U.S. Patent 2,871,218, granted in 1959.[46] Other progress in the 1960s and 1970s led to adoption of hard segments based upon diphenyl methane diisocyanate (MDI) and ethylene diamine (EDA) and/or propylene diamine (PDA).

Spandex currently produced reflects the work done in the past. Nearly all spandex fiber produced across the globe is based upon poly(tetramethylene ether glycol). Most spandex formulations are still based upon MDI and either EDA and/or PDA and are produced by a dry-spinning process from solutions of polymer in dimethyl acetamide or dimethyl formamide. The spandex market has been undergoing an expansion of ca. 7-8% yearly for a number of years and is

forecast to continue growing at this rate into the next millennium. The global spandex market in 1997 was ca. 200 million lbs/yr and in 1998, Lycra™ accounted for over half of the sales from DuPont's specialty fiber business unit (Figure 2-22).[74] Other significant spandex fiber producers include Asahi Chemical, BASF, Bayer, Globe Manufacturing, Tae Kwang, and Tongkook.

It is readily apparent, that given the magnitude of the spandex market, there is an enormous opportunity for substantial financial gain if significant enhancements to either the process or final product could be achieved. ARCO Chemical has recently developed catalyst technology that allows, for the first time, production of poly(propylene glycol) polyols suitable for use in high end elastomer production. These polyether polyols represent potential changes in the conventional spandex production process through both the replacement of

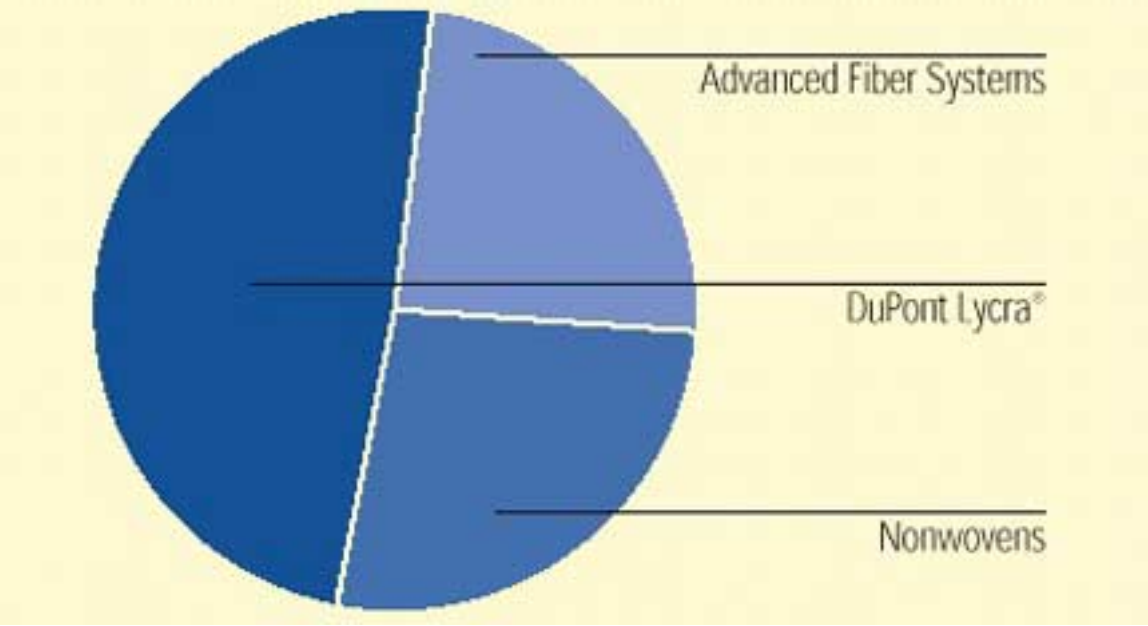

Figure 2-22. Lycra sales with respect to total sales of DuPont's Specialty Fibers business unit for 1998 (1998 DuPont Annual Report).[12]

poly(tetramethylene ether glycol) and by substantially increasing the throughput of the dry-spinning process.

Section 2-6: Methods

Small angle x-ray scattering (SAXS) and atomic force microscopy (AFM) can provide significant insights into the microphase separation characteristics of the linear segmented PUs and PUUs, as well as of other block copolymer systems. Dynamic mechanical analysis (DMA) or dynamic mechanical spectroscopy (DMS) is a technique sensitive to the changes in the thermal transitions that polymers undergo during heating. It also provides insight into the mechanical properties of polymers. Differential scanning calorimetry (DSC), while typically less sensitive to molecular transitions than dynamic mechanical analysis, will generally support those results and uniquely provides a view of the thermodynamic changes the polymers undergo upon heating (or cooling). Both dynamic mechanical analysis and differential scanning calorimetry allow for the estimation of some microphase separation characteristics, such as phase mixing, and can be used to illustrate that a given polymer exists as a block copolymer instead of a random copolymer. Wide angle x-ray scattering (WAXS) would initially appear to be inapplicable to this study since the poly(propylene glycol)s used in this study are atactic and believed to be non-crystallizable. However, PTMEG is crystallizable and it was desired to investigate the properties of PUUs with mixed soft segment types. Within the context of this, the strain-induced crystallization characteristics of these mixed soft segment materials may be partially characterized with WAXS. These same mixed soft segment materials also enable a study of the cold crystallization and melting behavior with DMA and DSC. Finally, birefringence and infrared linear dichroism enabled an assessment

of the molecular and segmental orientation characteristics of the poly(urethane-urea)s upon deformation.

Small angle x-ray scattering and AFM were applied extensively throughout this study. Simply put, those techniques make obtainable a vision of the microphase separated polymer which would be unobtainable otherwise. Alexander Pope stated many hundreds of years past, “Why has not man a microscopic eye”.[75] While man now possesses many *microscopic eyes* in his arsenal of investigative techniques, few are useful for the investigation of the morphology of poly(urethane-urea)s. Unlike many other block copolymers which exhibit microphase separation, the PUUs of this study are not readily imaged by transmission electron microscopy (TEM) or scanning electron microscopy (SEM).[76] Fortunately, SAXS allows for the terrain of the Lilliputian universe of PUUs to be inferred, and atomic force microscopy provides stunning visual confirmation of that inferred terrain. A variety of morphological features associated with microphase separated materials may be mathematically obtained through analysis of scattering results including interdomain spacing, domain size, degree of microphase separation, and interphase thickness. As stated, these parameters are obtained mathematically from the scattering results and it is therefore necessary that a terse review of some aspects of scattering theory germane to the current study be provided.

Section 2-7: Methods - Small angle x-ray scattering

A review of small angle x-ray scattering studies of polymers and particularly poly(urethane-urea)s cannot but leave one with the impression that we walk amongst giants. Dan Simmons states, "that as long as the task is both onerous and repetitive, the mind is not only free to wander to more imaginative climes, it actually flees to higher planes", and this truly must reflect the development of scattering theory and experiment.[77] Excellent and comprehensive reviews of small angle x-ray (and neutron) scattering exist and particularly useful, in context of the present work, is the review presented in the dissertation of Tyagi.[24,78-82]

In general, these discussions will be limited to the case of CuKα radiation which has a wavelength of 1.54Å. Briefly, when electromagnetic radiation interacts with the materials being investigated, a number of things may result (Figure 2-23). It is possible that the radiation may be transmitted, may remove a

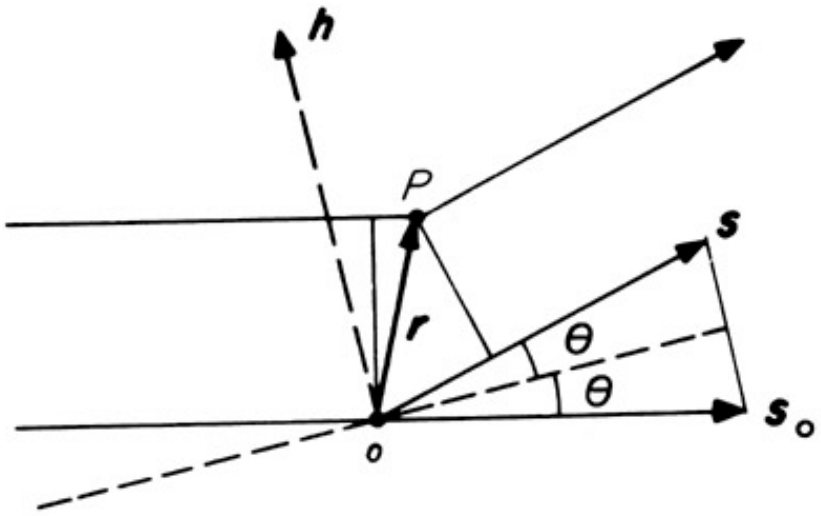

Figure 2-23. Scattering by two point centers.[11]

photoelectron with the resultant emission of fluorescent radiation, may result in characteristic Auger electrons, result in Compton scattering, or may result in Thomson scattering.[79] Compton scattering or incoherent scattering involves a change in wavelength and may be neglected in the development of small angle scattering theories.[83] Thomson or coherent scattering results from the fact that compared to the energy of the incident radiation, the electron binding energies of the target are weak, and therefore all target electrons will behave as free electrons.[83] When this is the case, released x-rays will have wavelengths

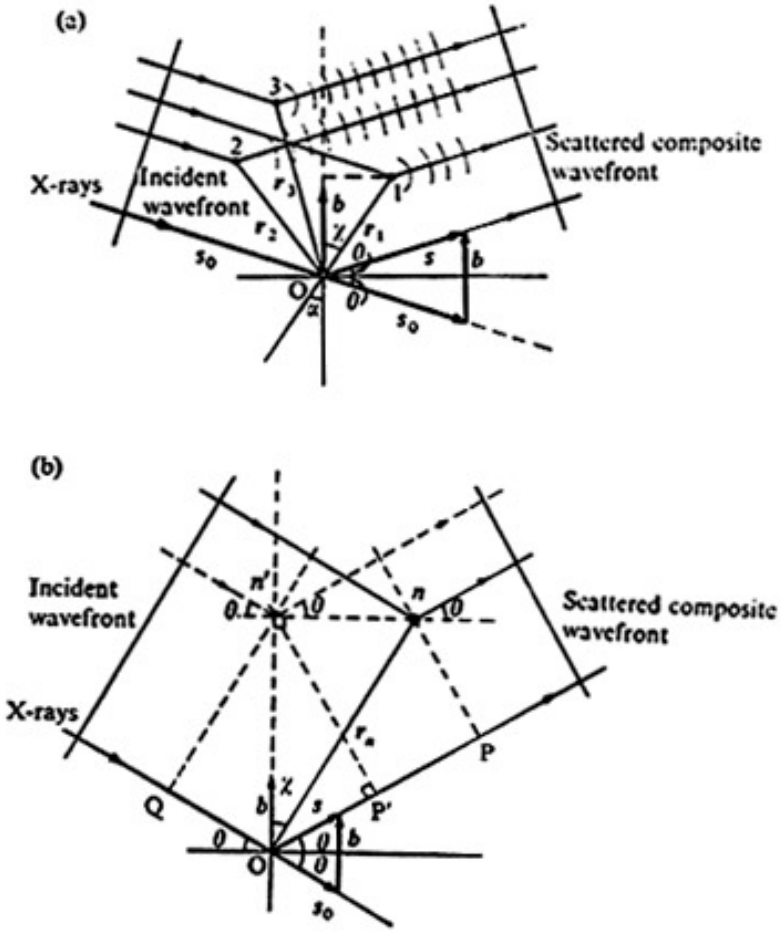

Figure 2-24. Schematic representation of scattering of x-rays by groups of electrons.[110]

identical to the incident radiation and will be of a phase related to that of the incident radiation (Figure 2-24) and for this reason these waves will then result in the phenomena of diffraction. The condition of coherence allows for the addition of amplitudes and the approximation of intensity as the square of the sum of amplitudes.[83] Porod has presented a superb development of the principles of scattering from which much of the following development was adapted.[83]

If one represents a secondary wave with the complex form, $\exp(i\cdot\phi)$, where ϕ is the phase, it may be shown with some development and with reference to Figure 2-23, that the phase will be take the form shown in Eqn. 2-4. This

$$\phi = -\boldsymbol{hr} \qquad (2\text{-}4)$$

where,
$\boldsymbol{h}$ is the vector in the direction of $\boldsymbol{s}-\boldsymbol{s_0}$, with magnitude $(4\pi\sin\theta)/\lambda$,
$\boldsymbol{r}$ is the path length between the origin and point P (Figure 2-23).

treatment will empoly the classical notation in which **h**, instead of **q**, is used to denote the vector in the direction of $\mathbf{s}-\mathbf{s_0}$. It is conceivable that all secondary waves in their complex form could be summed to obtain the amplitude, but this would prove an overwhelming task and is much simplified by the introduction of an electron density which will allow for the use of integration instead of summation. The electron density is simply the number of electrons encountered within a unit volume and is denoted as $\rho(\boldsymbol{r})$.[83] The amplitude may now be expressed in integral form (Equation 2-5) where it is shown as the Fourier transform of the electron density distribution. Recalling that the intensity is proportional to the square of the amplitudes, it is best obtained through application of the complex conjugate (Equation 2-6) of the integral shown above.

$$A(h) = \iiint dV \cdot \rho(r) \exp(-ihr) \tag{2-5}$$

where,
h is the vector in the direction of $\boldsymbol{s}$-$\boldsymbol{s_0}$, with magnitude $(4\pi\sin\theta)/\lambda$,
r is the path length between the origin and point P (Figure 2-23),
dV a volume element at position ***r***,
$\rho(\boldsymbol{r})$ is the electron density at position ***r***.

$$I(h) = \iiint\iiint dV_1 \cdot dV_2 \cdot \rho(r_1)\rho(r_2) \exp(-ih(r_1 - r_2)) \tag{2-6}$$

where,
h is the vector in the direction of $\boldsymbol{s}$-$\boldsymbol{s_0}$, with magnitude $(4\pi\sin\theta)/\lambda$,
$\boldsymbol{r_i}$ is the path length between the origin and point P_i (Figure 2-23),
$\boldsymbol{r_1}$-$\boldsymbol{r_2}$ is the relative distance between two points connected by $\mathbf{r_1}$ & $\mathbf{r_2}$,
$\rho(\boldsymbol{r_i})$ is the electron density at position $\boldsymbol{r_i}$.
dV_i a volume element at position $\boldsymbol{r_i}$,

The resulting expression is rather forbidding at first glance, but can be simplified through application of the concept of auto-correlation or convolution square, where when ***r*** = ($\boldsymbol{r_1}$ –$\boldsymbol{r_2}$) is taken to be a constant, the convolution square may be defined (Equation 2-7). This function has the property that for each pair of electrons separated by the relative distance ***r***, a point will exist in a contrived space.[83] The distribution of these points is the auto-correlation (Equation 2-7) and by necessity will show a center of symmetry due to the double counting with respect to ***r*** and ***–r***.

$$\tilde{\rho}^2(r) \equiv \iiint dV_1 \rho(r_1)\rho(r_2) \tag{2-7}$$

where,
$\rho(\boldsymbol{r_i})$ is the electron density at position $\boldsymbol{r_I}$,
dV_i a volume element at position $\boldsymbol{r_i}$,
$\tilde{\rho}^2(r)$ is the auto-correlation or convolution square,
r is defined as ($\boldsymbol{r_1}$ –$\boldsymbol{r_2}$) and is taken to be a constant.

Applying the result of equation 2-7 to equation 2-6 will yield an expression for the integration over the fictitious space described above (Equation 2-8), which

$$I(h) = \iiint dV \cdot \tilde{\rho}^2(r) \cdot \exp(-ihr) \qquad (2\text{-}8)$$

where,
I(h) is the intensity distribution over h,
dV is a volume element over the space described above,
$\tilde{\rho}^2(r)$ is the density of points in this space,
r is the distance between two points, (***r*****$_1$** **–*****r*****$_2$**) ,

is again a Fourier transform, in this case relating the intensity distribution to the structure of the object as defined by $\tilde{\rho}^2(r)$. Two restrictions, which are applicable to many encountered systems will greatly further development of small angle scattering theory.[83]

The first of these restrictions is that the material being investigated is isotropic in a statistical sense. A consequence of this restriction is that the distribution, $\tilde{\rho}^2(r)$, will depend only on the magnitude of ***r*** which will allow replacement of the phase factor, exp(-i***hr***) by its average, sin(hr)/hr. The second restriction is that no long range correlation exists between regions of similar electron density within the material which implies that electron densities become independent of one another. Within context of this second restraint, the electron densities may be replaced by a mean electron density, and ultimately, Equation 2-8 may be rewritten in terms of the restrictions placed upon the system (Equation 2-9).[82] Within Equation 2-9 are two terms that have not yet been

$$I(h) = 4\pi \overline{\Delta\rho}^2 \int_0^\infty \gamma(r) \cdot r^2 \cdot \frac{\sin(hr)}{hr} dr \qquad (2\text{-}9)$$

where,
$\overline{\Delta\rho}^2$ is the mean square electron density fluctuation,
γ(r) is the correlation function.

introduced, the mean square electron density fluctuation and the correlation function. The mean square electron density fluctuation is derived from considerations stemming from the use of the mean electron density and is defined in Equation 2-10. It is readily apparent from Equations 2-9 and 2-10, that

$$\overline{\Delta\rho}^{2}(r) = \left(\rho(r) - \overline{\rho_m}\right)^2 = V \cdot \gamma(r) \qquad (2\text{-}10)$$

where,
ρ_m is the mean electron density,
V is the illuminated volume of the material,
$\gamma(r)$ is the correlation function.

without deviation from the mean electron density, the scattered intensity will be zero. The mean square electron density fluctuation will therefore act as a contrast factor in the scattering analysis. The correlation function is somewhat less easily described, though simply put, it is a functional representation of spatial correlation of local fluctuations in the electron density or alternatively represents the degree of inhomogeneity in $\rho(r)$.[84] The correlation function is a function of the probability that a stick of length r will have both ends in regions of identical electron density and is found by taking the inverse Fourier transform of the scattering intensity distribution (Equation 2-11).[85] The special case of

$$\gamma(r) = \frac{1}{2\pi^2 V}\int_0^\infty h^2 I(h)\frac{\sin(hr)}{hr}\,dh \qquad (2\text{-}11)$$

where,
V is the illuminated volume of the material,
I(h) is the scattered intensity.

$$Q = \int_0^\infty h^2 I(h)\,dh = \overline{\Delta\rho}^{2} V \qquad (2\text{-}12)$$

Equation 2-11 when r = 0, (i.e. a limiting value) yields a value known as the invariant, Q (Equation 2-12). The correlation function may also be represented in

one dimensional form (Figure 2-25) and it can be seen that maxima are indicators of periodicity within the investigated material.[82] Similarly, maxima in the plot of the scattered intensity as a function of the scattering vector, h (or s) will provide much the same information. The majority of the SAXS analysis undertaken in this study employs this latter, somewhat more simplistic method.

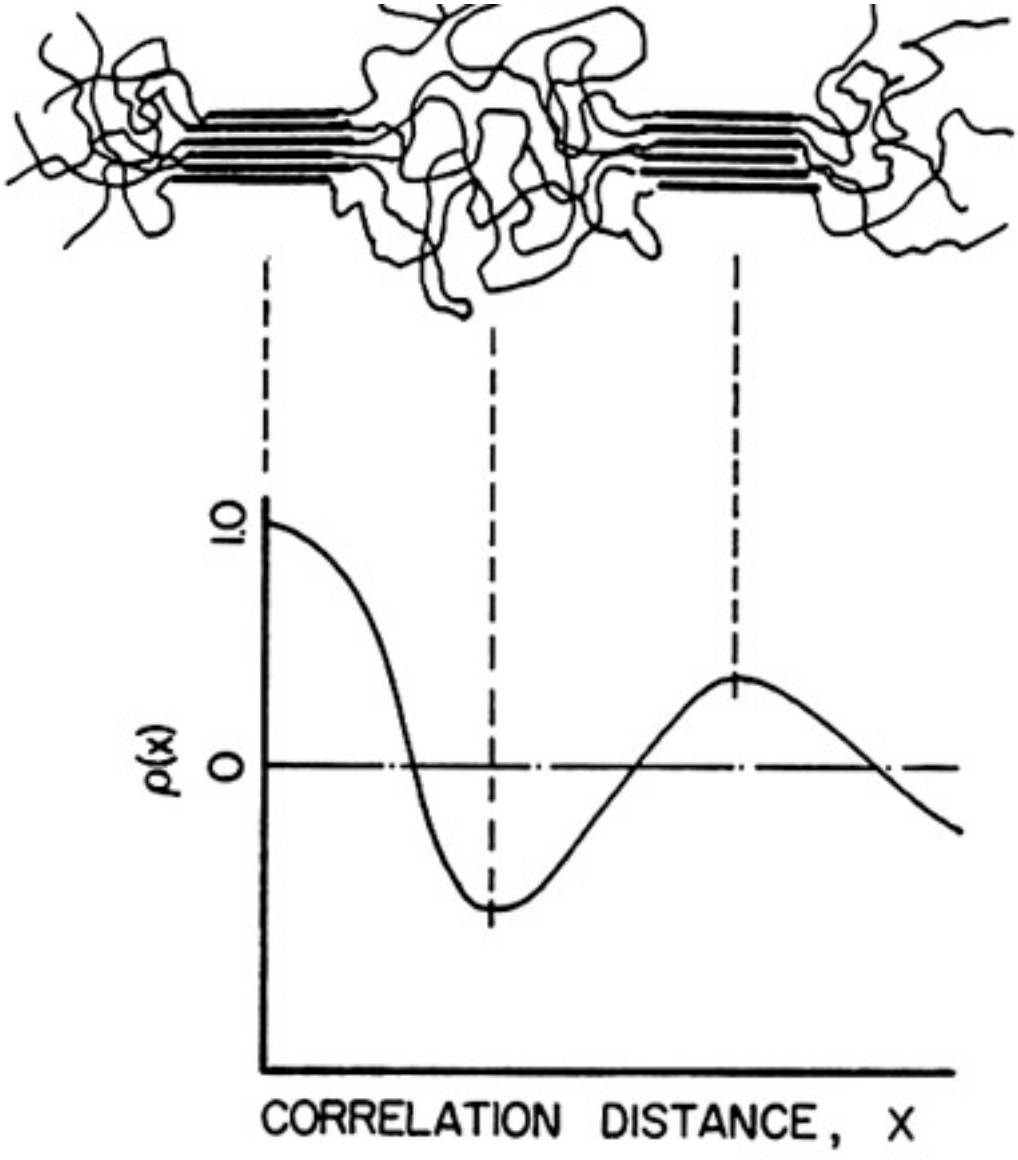

Figure 25. Schematic of one dimensional correlation function.[8]

Different regions of the scattering curves are useful for inferring information about different morphological aspects of the material being studied. The intensity of the scattering curve reflect the extent or degree of phase separation and the breadth of the intensity distribution is an indicator of the inhomogeneity sizes present within the material.[83,86] More importantly in the current work, the interdomain spacing may be estimated from the position of maxima in the scattering curve and the tail of the scattering curves contain information regarding the interphase thickness between the hard domains and soft phase.[82,87] Before, any information is extracted from the scattering curves, there are some aspects of data treatment which must be considered.

The scattering curves obtained from the SAXS experiments are obtained using a Kratky type camera that provides slit-smeared results. Pin-hole radiation sources, avoid the added difficulty of smeared data, but are typically lower in available intensity.[88] Slit collimating systems (Figure 2-26) improve the impinging intensity but also detect intensity from scattering angles other than that of the primary beam.[88] Mathematically, this “smearing” may be removed via

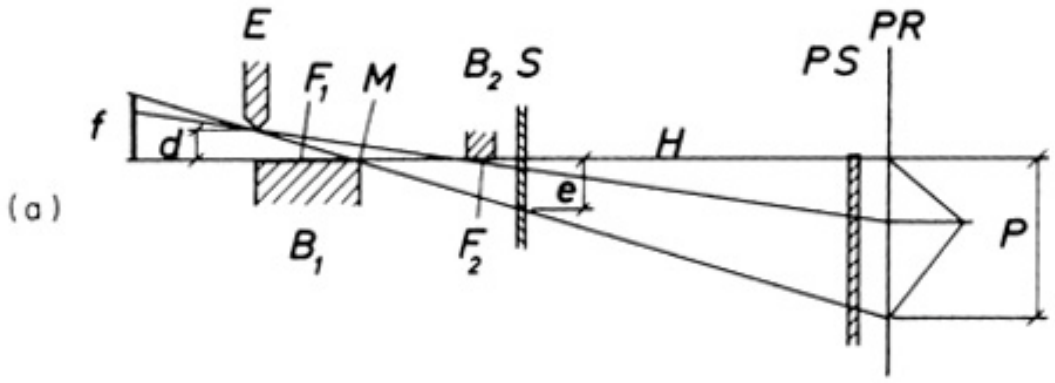

Figure 2-26 Block collimation system for a Kratky camera.[4]

mathematical manipulation of the data set, but through such procedures additional sources of error may be introduced. As a rule, desmearing shifts the maxima in the scattering curves to higher angles, which then correspond to lower spacings.[24,89] Rather than desmear the data in an attempt to mimic pin-hole collimated results, it will simply be acknowledged that the interdomain spacings obtained from SAXS will generally be somewhat larger than in reality and it will be accepted that the peaks in the scattering profile will appear to be less sharp than in the desmeared case.

Another drawback of slit systems is that there will exist secondary scattering off of the slit, which will be evident in the small angle region. This secondary scattering is known as parasitic scattering. Block collimating systems, such as the one used in this study, provide slit smeared data with diminished aspects of parasitic scattering, but the resulting scattering curves are limited to the scattering on one side of the primary beam.[88] Still, some limited parasitic scattering must be accounted for in data treatment and subtracted from the observed intensity.

It is often preferable to obtain the absolute scattering intensity profile, which is simply the ratio of the scattered intensity to that of the main beam. Kratky has reviewed a number of procedures for obtaining the absolute intensity including Luzzati's use of filters to attenuate the main beam, use of primary standards for which the ratio of scattered and primary intensity is determinable theoretically, and the use of a moving slit device.[88,90] Kratky also presents a procedure by which the absolute intensity may be obtained through the use of a

secondary standard, in this case, Lupolen.[88] Lupolen, specifically Lupolen 1811M of the Badische Anilin & Sodafabrik, is a thin slab of polyethylene for which the absolute intensity at a specific scattering angle has been determined. Absolute intensities are typically obtained in the current work via the Lupolen secondary standard procedure of Kratky. It has been determined that as a standard, Lupolen is insensitive to repeated exposure to x-rays and that scattering power shows a +1% / 1ºC temperature dependence.[91-93] While Kratky has shown a minor temperature dependence in the calculation of absolute intensities using a Lupolen secondary standard, laboratory temperature variations have not been accounted for.

Finally, in the analysis of interphase thickness, it will be important to account for thermal density variations which is also known as background scattering.[84] Porod's law, which will be discussed in more detail shortly, may be modified to include the effect of background scattering (Equation 2-13). The

$$I_{obs}(s) = I_P(s) \cdot H^2(s) + I_B(s) \qquad (2\text{-}13)$$

where,
$I_{obs}(s)$ is the observed, scattered intensity
$I_P(s)$ is the scattered intensity due to the polymer,
$I_B(s)$ is the intensity of background scattering,
$H^2(s)$ is the Fourier transform of a smoothing function.

additional term, $I_B(s)$, describes the contribution of background scattering, the functional form and its determination have been addressed by researchers such as Bonart, Ruland, and Vonk.[24,94-96] Briefly, Bonart assumes that the background scattering intensity is independent of angle while Ruland and Vonk's treatments include an aspect of angular dependence. Vonk, as well as Koberstein and

Stein, reported that treatment of background intensity did not significantly affect the estimation of the interphase thickness parameter, σ, but Tyagi found for segmented poly(siloxane-urea)s with small interphase thicknesses, the choice of background treatment had significant effect.[82,96-97] Bonart's method of constant background across the entire angular range was found to be inappropriate for the materials being examined in the current work. The method of Vonk, where the functional form of the background is expressed in Equation 2-14, to obtain acceptable correction of the background is used throughout this

$$I_B(s) = C' + b's^n \quad (2\text{-}14)$$

where,
C' is a graphically obtained parameter, the intercept,
b' is a graphically obtained parameter, the slope,
n is a constant chosen arbitrarily to obtain a good fit of the linear region.

study. This method, is graphical in nature, requiring a plot of observed intensity versus the scattering vector raised to an arbitrary power, n. The exponent, n, is chosen to obtain a good fit of the linear region. n = 4 was generally found to work well in the present study. The parameters b' and C' are the slope and intercept respectively of the aforementioned plot (Figure 27A). Using the form of the background suggested by Vonk, the function $I_B(s)$ is determined and subtracted from the experimentally observed background to obtain the background corrected scattering intensity profile.[96]

While differences in the magnitude of the intensity and breadth of the intensity distribution are used qualitatively throughout the study, there are two parameters that are quantitatively compared. Those are the interdomain spacing, d, and the interphase thickness, σ. In general, the interdomain spacing

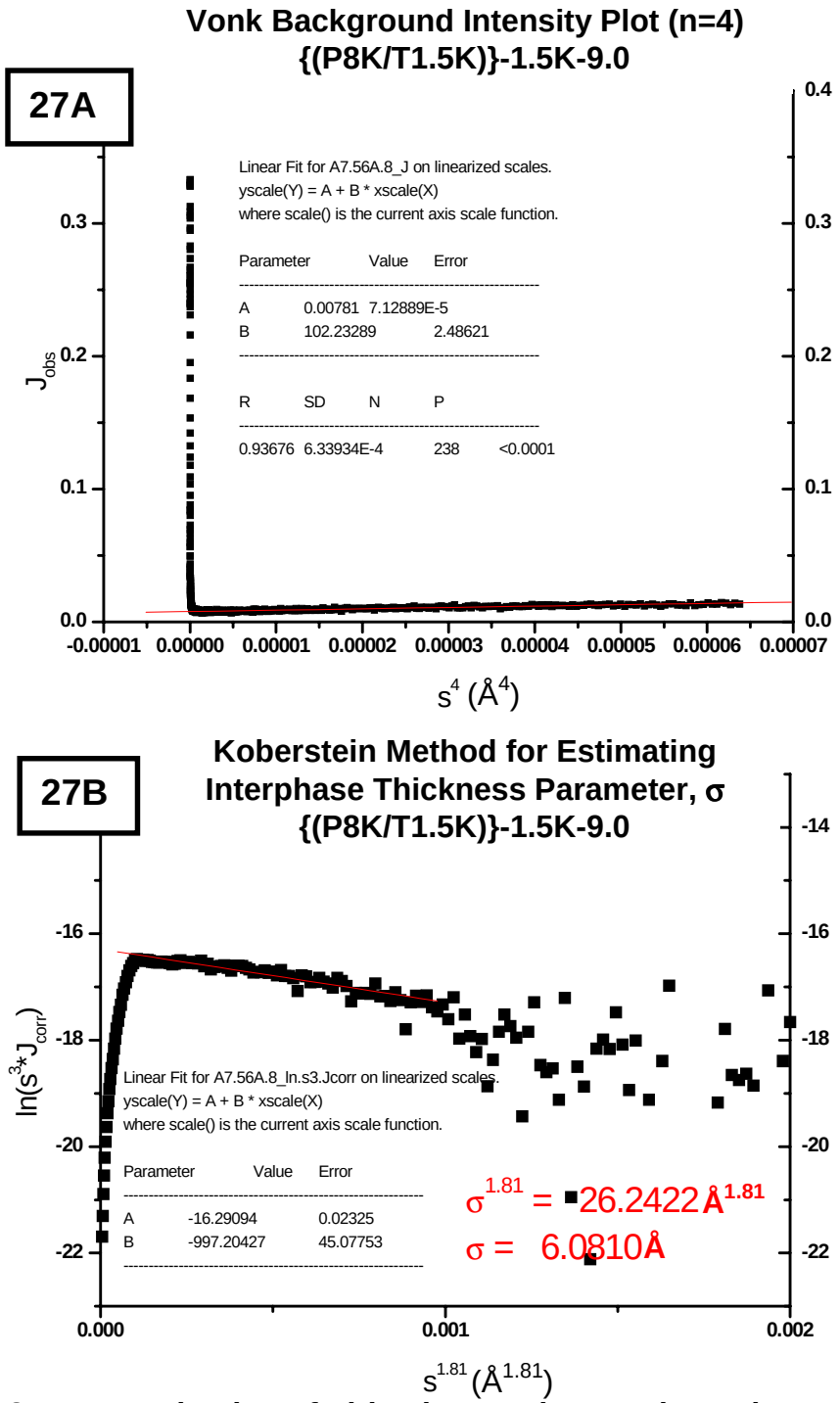

Figure 2-27. Determination of A) background scattering using a Vonk plot and B) interphase thickness using Koberstein's method.

is obtained from either a maximum in the correlation function or through the use of the relation developed by W. L Bragg (Equation 2-15.) which relates the

$$\frac{1}{d} = \frac{2\sin\theta}{m\lambda} \qquad (2\text{-}15)$$

where,
m is, for the case of constructive interference, is any integer,
λ is the wavelength of the scattered radiation,
θ is one half of the Bragg angle for radial scattering in transmission,
d is the center-to-center distance of two scatterers.

scattering angle to the reciprocal of the distance between scattering particles.[97] It is not wholly appropriate to use Bragg's Law with slit-smeared data, but it will still provide a useful measure of the interdomain spacing of a microphase separated material.[82] Essentially, a maximum is located in the absolute intensity scattering profile. The reciprocal of the vertical coordinate of the maximum yields an estimated value for the interdomain spacing. This procedure is schematically represented for a microphase separated system in Figure 2-28.

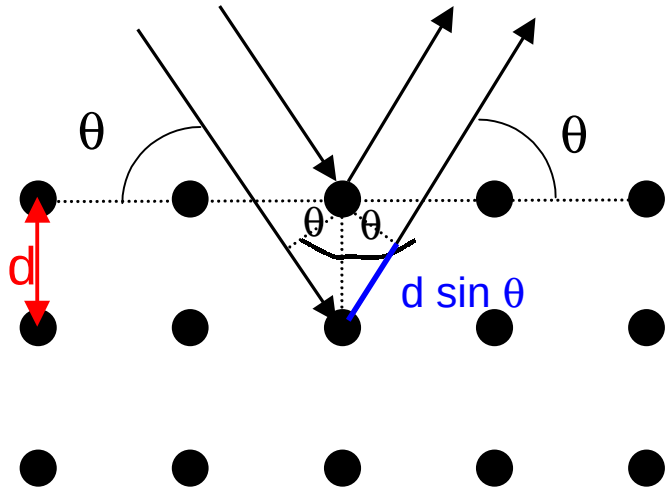

Figure 2-28. Bragg condition.

The second quantitative measure of the microphase separation characteristics measured with small angle x-ray scattering is that of the interphase thickness parameter, σ. Expanding the correlation function as a power series and substituting it into the expression shown in Equation 2-9, yields

a function which may be integrated to obtain a series form of the intensity distribution (Equation 2-16).[82] It is readily apparent from this series form of the

$$I(s) = \frac{\overline{\Delta\rho}^2 S}{8\pi^3 s^4} + \frac{A}{s^6} + \frac{f(u,s)\cos(u)}{s^3} + \frac{g(u,s)\sin(u)}{s^3} + \ldots \qquad (2\text{-}16)$$

intensity function that as the scattering vector increases, the second term will contribute little to the overall value of the intensity, and that subsequent pairs of terms will tend to cancel one another. This leaves, for cases of large scattering vector, s, only the first term to provide any meaningful contribution to the intensity profile. Expressing this as a limit (Equation 2-17), reveals that in an ideal two phase system a constant value should be obtained for the product of the intensity and s raised to the fourth power. This constant, K_P, is known as Porod's

$$\lim_{s\to\infty}(I(s)) = \frac{\overline{\Delta\rho}^2 S}{8\pi^3 s^4} = \frac{K_P}{s^4} \qquad (2\text{-}17)$$

where,
s is the magnitude of the scattering vector,
$\overline{\Delta\rho}^2$ is the mean square electron density fluctuation,
K_P is the Porod constant.

constant. One of the conditions mentioned in the development of Equation 2-17 was that an ideal two phase system existed, which more explicitly implies that the boundaries between the phases are sharp, and that there is no phase mixing.[98] If such is the case, then graphing the product of the intensity and fourth power of the scattering vector versus either s^2 or s should result in a constant being obtained for the value of $I \cdot s^4$.[83] When a constant value is not obtained, as is the case for most microphase separated materials, it will be exhibited as either

negative or positive deviations from the ideal behavior. The presence of the interphase between hard domains and soft phase will result in a negative deviation since there will be more material with electron density near that of the mean electron density. On the other hand, positive deviations may result from the isolated mixing of hard segments within the soft phase (and vice versa). Ruland proposed that an ideal two phase system may be related to a real two phase system (Equation 2-18) through convolution of the ideal electron density

$$\rho_{real}(r) = \rho_{ideal}(r)*h(r) \quad (2\text{-}18)$$

where,
h(r) is a smoothing function describing the interphase.

profile with a smoothing function which describes the change in electron density across the interphase region.[95] Application of the real electron density profile, as derived from the ideal, yields an expression for the real intensity in terms of the ideal and the Fourier transform of the smoothing function (Equation 2-19).

$$I_{real}(s) = I_{ideal}(s) \cdot H^2(s) \quad (2\text{-}19)$$

where,
$H^2(s)$ is the Fourier transform of the smoothing function, h(r).

Conveniently, it was shown by Guinier that for slit-smeared data, the real intensity was expressible as shown in Equation 2-20.[99] A number of researchers, including Ruland, Bonart, and Koberstein, have developed expressions for the

$$I_{real}(s) = \frac{K_P'}{s^3} H^2(s) \quad (2\text{-}20)$$

where,
K_P' is the equal to $K_P \cdot (\pi/2)$,
$H^2(s)$ is the Fourier transform of the smoothing function, h(r).

function $H^2(s)$ when a sigmoidal gradient is assumed and slit smeared data are available (Table 2-10).[87,94-95,100] The function $H^2(s)$ contains the interphase thickness parameter, σ, which is readily attainable via graphical methods (Table 2-10). Within this work, the methods of Bonart and Koberstein are applied exclusively (Figure 2-27B).

Table 2-10. Forms of $H^2(s)$, assuming a sigmoidal gradient across the interphase region.[51-54]

Function Name	Function Form
Bonart	$\exp(-4\pi^2\sigma^2 s^2)$
Ruland	$(1-8\pi^2\sigma^2 s^2)$
Koberstein	$\exp(-38(\sigma s)^{1.81})$
Exponential	$\exp(-8\pi^2\sigma^2 s^2)$
Helfand	$\left(\sqrt{12}\pi\sigma s\right)^2 \cos\mathrm{ech}^2\left(\sqrt{12}\pi\sigma s\right)$
Roe	$3.3\left(\sqrt{12}\pi\sigma s\right)^{1.8} \exp\left(-1.9\pi\sigma s\right)s^3$

Section 2-8: Methods – Atomic Force Microscopy

Other than SAXS, the technique which most directly provides information regarding the microphase separation characteristics of the linear segmented block copolymers and the poly(urethane-urea)s in particular, is AFM. The history of AFM is not nearly so extensive as that of small angle x-ray scattering, but has proven to be quite fecund in its development.[101] Atomic force microscopy is a specific member of the family of scanning probe microscopies (SPM). The first member of this family, scanning tunneling microscopy (STM) was born in 1981 and was used to obtain topographical images of conducting surfaces with potential atomic resolution capabilities (Figure 2-29)[101] A feedback loop including

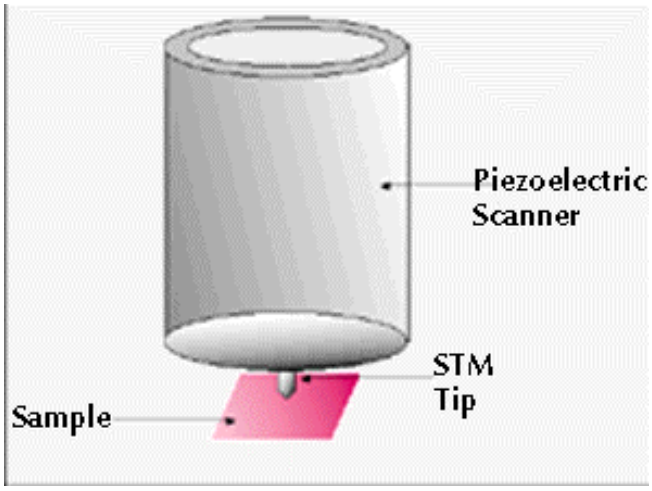

Figure 2-29. Schematic of Scanning Tunneling Microscope.[55]

the tunneling current, allowed for use of a precision piezoelectric motion device to image the surface with sub-angstrom accuracy. In some aspects, it was similar to conventional profilometers with the significant difference that it sampled the surface of a material in a raster pattern to obtain an image of the surface with x,y, and z coordinates, whereas the profilometers obtained only a single line

across the surface. While being a significant advance in surface imaging, it was limited by the requirement that the sample be conductive.[101] The first atomic force microscope overcame this limitation by attaching the sharp probing tip to a cantilever which is held against the sample surface by a very low force which is of the magnitude of interatomic forces. Deflections of the cantilever as it was drawn across a sample surface were detected and used to determine the surface topography (Figure 2-30A).[101] This technique is specifically known as contact mode atomic force microscopy. While allowing for non-conductive samples to be imaged, there existed the potential to damage the surface and/or tip while dragging the tip across the material. This limitation was of particular concern when polymers and biological systems were being investigated.

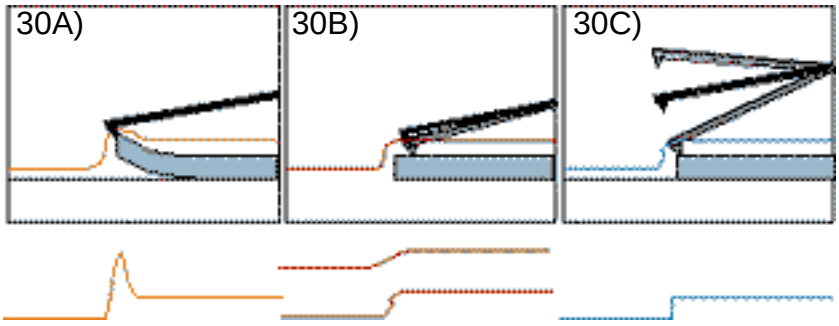

Figure 30. General schematic of AFM probe-tip/sample interactions: A) contact, B - non-contact, and C - tapping mode AFM.[59]

The potential for sample damage was overcome by the development of TappingMode™ atomic force microscopy.[102] In TappingMode™ AFM the cantilever is oscillated near its resonance frequency while in air. When the oscillating cantilever approaches the surface of the sample, the amplitude of oscillation decreases. A feedback loop will then maintain the decreased amplitude while the tapping tip is rastered across the sample (Figure 2-31).[102]

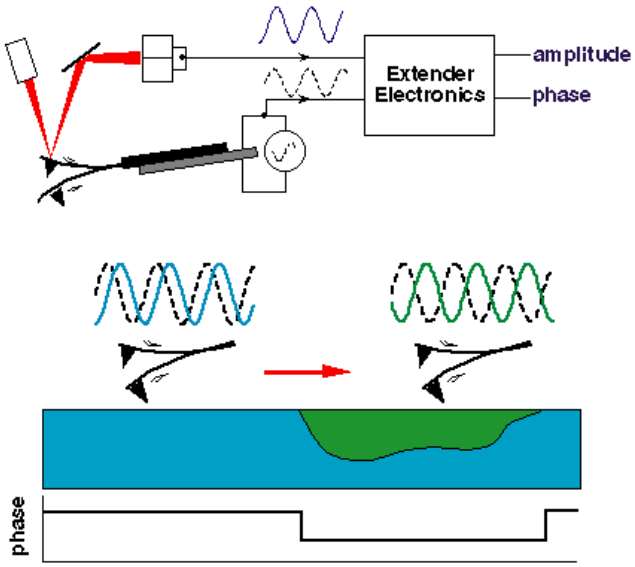

Figure 2-31. Tapping mode AFM used to obtain a phase image.[59]

TappingMode allows for imaging of soft materials, materials with thin films of absorbed water and gas, and a number of biological systems that would be otherwise unimagable. In addition to topographical features, TappingMode AFM may also provide a phase image, derived from the phase of the cantilever oscillation, which may register variations in composition, viscoelastic properties, adhesive properties, and frictional properties.[103] Of particular relevance to the current investigation, is the fact that differences in the surface modulus may be detected through phase imaging, thus allowing for vivid images of microphase separation materials (Figure 2-32) even on atomically flat surfaces.[103] This is of course dependent on there being a difference in the surface moduli of the two phases in the polymer being investigated. This difference in moduli is in turn dependent upon the test temperature in respect to the glass transition temperatures of the two phases.

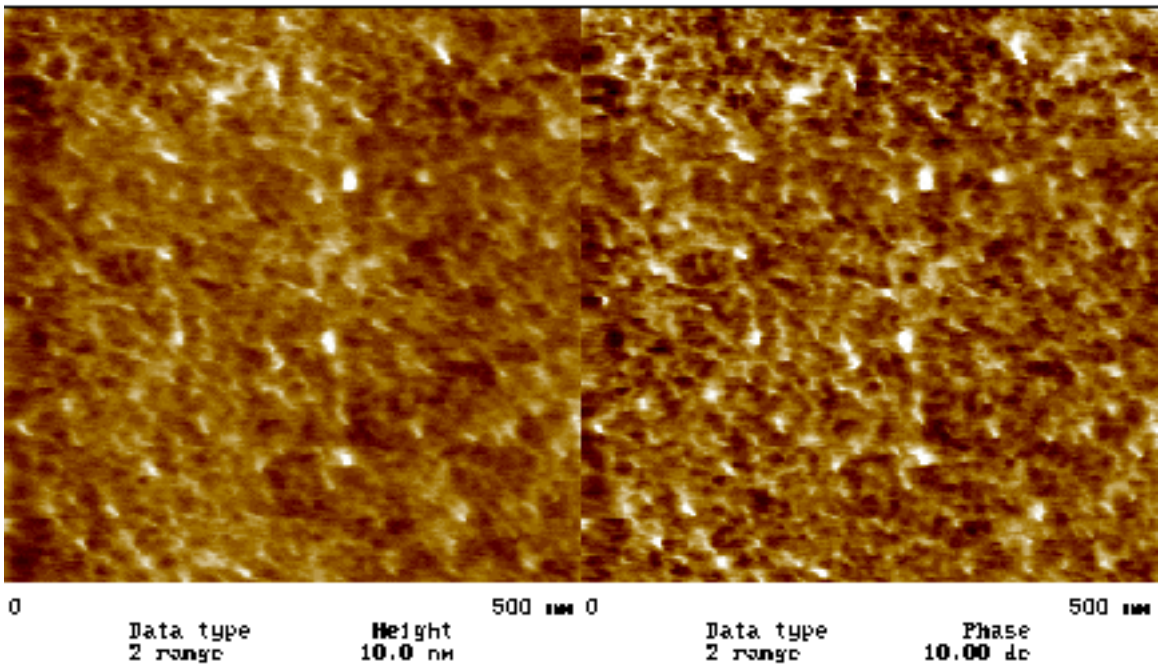

Figure 2-32. AFM Tapping mode height (left) and phase (right) images of PTMEG-based poly(urethane-urea) with 9wt% HS, where, for the phase image, darker regions are comprised of soft segment material and lighter regions are composed of hard segment material.

While AFM is often considered to be a surface characterization technique, it is reasonable to posit that the surface microphase characteristics will reflect those of the bulk. This is a reasonable assumption when one considers that the blocks of poly(urethane-urea)s are more numerous and smaller than those of copolymers such as Kraton (which can have block weights of ca. 50,000 g/mol), and that these shorter block lengths restrict the formation of substantial differences between surface and bulk morphology. However, in the context of surface characterization microscopies, Table 2-11 provides a comparison between optical microscopy, scanning electron microscopy, and scanning probe microscopy and it is readily seen that SPM provides considerable investigative advantages that optical microscopy and SEM cannot provide.[104] Even in the

Table 2-11. Characteristics of Common Techniques for Imaging and Measuring Surface Morphology (From Digital Instruments).[63]

	optical microscope	SEM	SPM
sample operating environment	ambient, liquid, vacuum	vacuum	ambient liquid, vacuum
depth of field	small	large	medium
depth of focus	medium	small	small
resolution: x,y	1.0μm	5 nm	0.1-3.0 nm
resolution: z	N/A	N/A	0.01 nm
magnification range	1X-2x10^3X	10X-10^6X	5x10^2X-10^8X

present study, it is noted that SPM remains largely a surface or near surface technique, while SAXS probes both the surface and bulk of a sample.

Section 2-9: Methods – Dynamic mechanical analysis

Dynamic mechanical analysis (DMA), dynamic mechanical spectroscopy as it is sometimes known, while not providing a vivid image of microphase separation as AFM does, does provide useful insights into the thermo-mechanical bulk properties of block copolymers. Unlike conventional creep and stress relaxation experiments where a polymer sample is subjected to a step input of stress or strain, dynamic mechanical analysis applies an oscillatory stress or strain input and tracks the system's response as a function of frequency instead of time.[105-107] The complex Young's modulus, E*, (Equation 2-21) that consists of contributions of a storage modulus, E', and a loss modulus E", is measured. This complex modulus reflects the inherent viscoelastic nature of polymers, where stresses and strains will be out of phase with one another

$$E^* = E' + iE'' \qquad (2\text{-}21)$$

where,
E* is the complex Young's modulus,
E' is the storage modulus,
E" is the loss modulus.

(Figure 2-33).[107] The storage modulus is a quantification of the energy stored elastically by the material upon deformation. The loss modulus, on the other hand, is a measure of energy that is dissipated as heat during deformation. The two moduli will show distinct differences in behavior as functions of temperature. From the ratio of the loss and storage moduli, a third parameter, tan δ or the loss tangent or factor (Equation 2-22), is obtained. The storage modulus generally reflects the behavior of the Young's modulus obtained from static and slow transient measurements. The loss modulus and loss tangent are useful

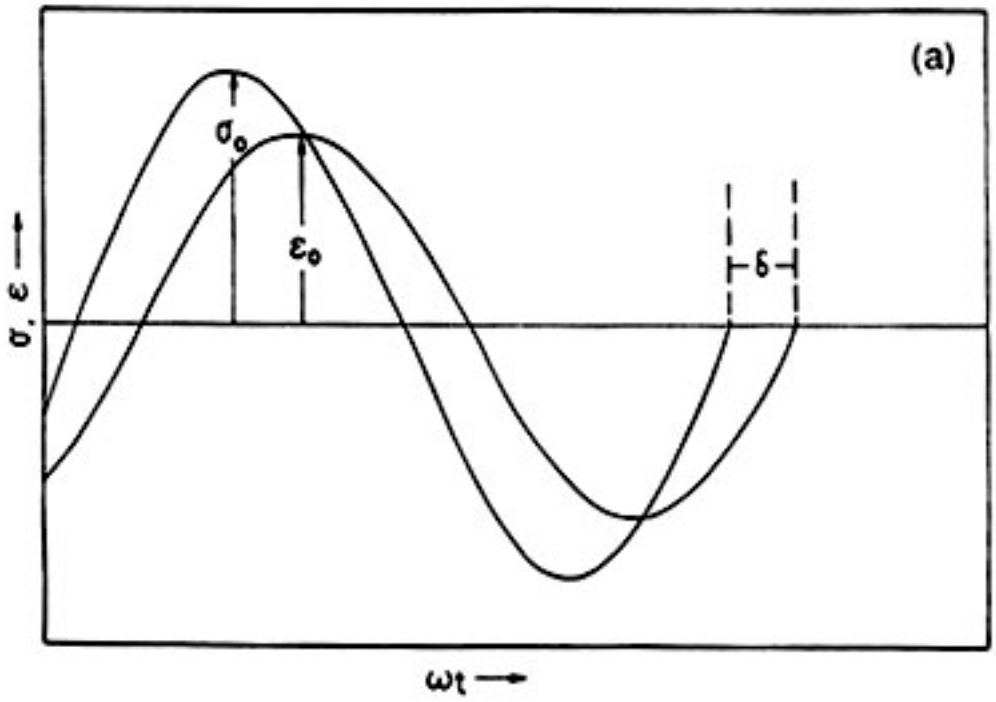

Figure 2-33. Stress and strain in DMA and phase offset delta.[66]

$$\tan\delta = \frac{E''}{E'} \qquad (2\text{-}22)$$

where
tan δ is measure of the dissipative properties of the polymer,
E' is the storage modulus, and
E" is the loss modulus.

indicators of a material's ability to internally dissipate energy under the test conditions. For this reason, peaks in the tan δ plots are often referred to as damping peaks. The greater the peak, the greater the polymers ability to "damp" or dissipate noise and vibrations of the appropriate frequency.[106-107]

Dynamic mechanical analysis is sensitive to the various transitions that a polymer will undergo as a function of changing temperature.[107] For instance, in poly(urethane-urea)s based upon PTMEG, DMA can detect as a function of increasing temperature the so-called crankshaft motion of backbone groups of

methylenes, the soft segment glass transition, cold crystallization of the soft segment, melting of soft segment crystallites, and the softening of the hard segments.[39,72,108] These transitions span a temperature range from ca. -160ºC to 200ºC. The behavior of these transitions can provide useful clues concerning the morphological, compositional, and microphase separation state of the polymer. One striking example of the use of dynamic mechanical analysis was its early use to ascertain that a given copolymer was a block copolymer instead of a random copolymer. The Fox equation (Equation 2-23), developed for random copolymers, suggests that a single glass transition temperature will be exhibited by a random copolymer.[106] This glass transition of the random copolymer will be

$$\frac{1}{T_g} = \frac{M_1}{T_{g1}} + \frac{M_2}{T_{g2}} \qquad (2\text{-}23)$$

where
T_g is the predicted glass transition temperature of a random copolymer,
M_i is the weight fraction of component i, and
T_{gi} is the glass transition of the homopolymer i.

intermediate between the glass transition temperatures of the homopolymers of the copolymer components. Tobolsky and Cooper demonstrated that microphase separated block copolymers on the other hand will show multiple glass transition temperatures, one for each type of block (Figure 2-34).[46] It is apparent that as the block sizes decrease, the glass transition behavior of the block copolymer will begin to resemble that of the random copolymers.

Before closing the review of dynamical mechanical analysis there are a few final points to be made. The nature of the test requires that the sample

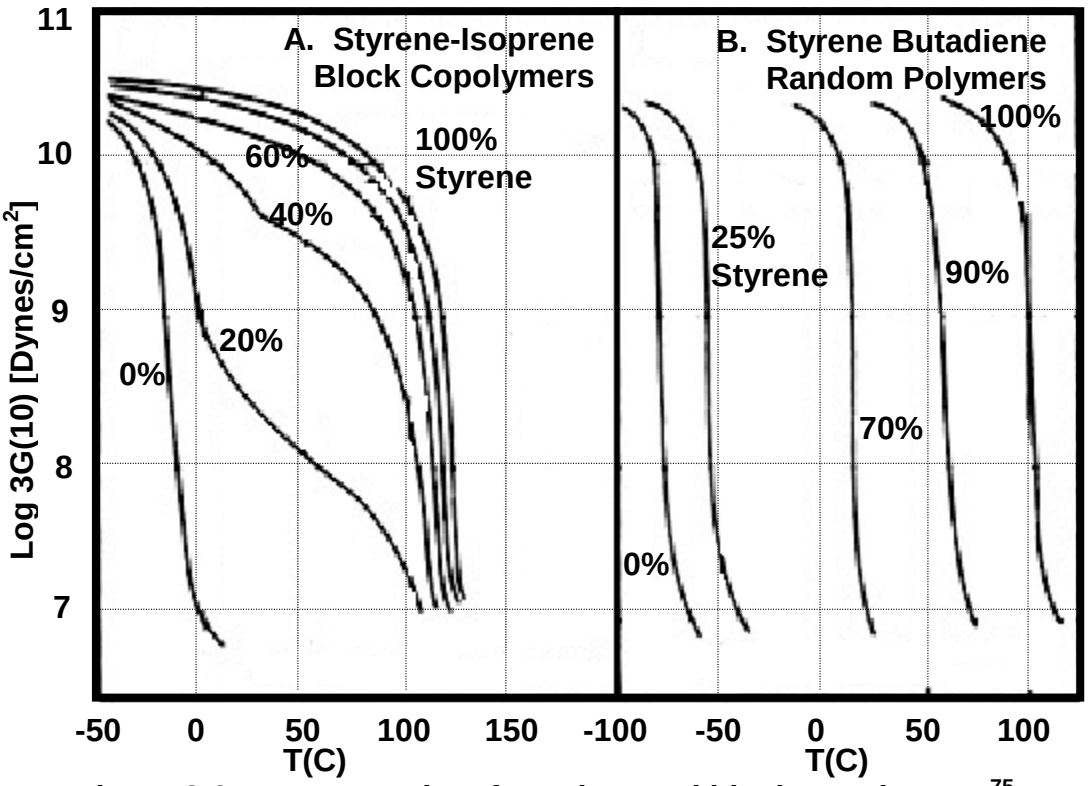

Figure 2-34. DMA results of random and block copolymers.[75]

maintain its integrity over the temperature range being investigated. This precludes the use of DMA to investigate changes above the softening of the hard segments of non-crosslinked systems. It is possible to examine such materials if they are braid supported in a torsion pendulum. Similarly, it is not of great value for the investigation of thermal degradation characteristics, since thermal degradation may imply, amongst other possibilities, chain scission, which leads to loss of sample integrity, and crosslinking which appreciably alters the elastomeric properties of the sample. Finally, the profiles obtained are dependent upon the choice of test frequency and indeed, use of multiple frequencies will permit calculation of activation energies of various transitions. In earlier literature, the frequencies of strain input will often be seen such as 3.5, 11,

35, and 110 Hz. These were typically obtained with Rheovibron instruments, which were at that time the only ones commercially available, on which the frequency choices were limited due to considerations of mechanical resonance within the instrument.[107] Recent literature shows that the most common frequency choice is 1 Hz, largely due to 1 Hz being the designated standard frequency of ISO and ASTM methods, such as ASTM D 2231 “Rubber Properties in Forced Vibration”.[109-110] Throughout the present work, a frequency of 1 Hz was used exclusively.

Section 2-10: Methods – Differential scanning calorimetry

Differential scanning calorimetry (DSC) and differential thermal analysis (DTA) are two of the most prevalent methods of thermal analysis in polymer science and both provide similar information. Historically, differential thermal analysis is the older of the two methods and will be briefly reviewed first in order to help elucidate the advantages of differential scanning calorimetry.

Differential thermal analysis (schematically shown in Figure 2-35) involves comparison of sample temperature to the temperature of a reference material during a uniform heating process.[106] Differences in the two materials', sample

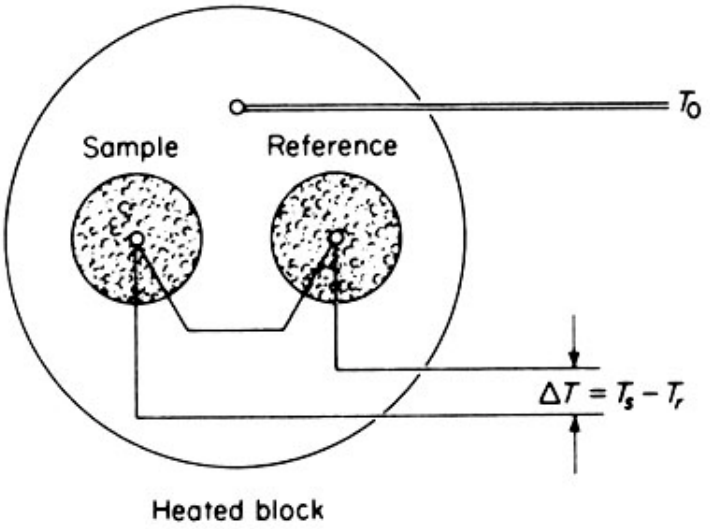

Figure 2-35. DTA schematic.[69]

and reference, heat capacity result in a difference of temperature, ΔT. The temperature difference, ΔT, is sensitive to transitions such as the glass transition, as well as endo- and exo-therms due to crystallization, melting, and chemical reaction.

Differential scanning calorimetry on the other hand, maintains the sample and reference at the same temperature through varying the heat flow to each. When the differential heat flow supplied is plotted as a function of temperature, it is possible, after normalizing with the sample mass, to readily obtain enthalpic information, such as the heat of fusion.[106] There are a number of features and physical parameters that DSC provides (Figure 2-36). The heat capacity change upon passing through the glass transition may be obtained by extending the linear regions before and after the glass transition and noting the difference between these two lines at the midpoint of the glass transition.[107] The glass transition may be characterized by the onset temperature of the transition and the glass transition temperature, which is taken as the midpoint of the transition region or obtained from the inflection point in the glass transition region of the DSC plot. Within this study, the glass transition temperature as reported from DSC will be obtained from the inflection point of the glass transition. Similarly, cold crystallization is characterized by both the onset temperature and the temperature associated with the crystallization peak. The integrated area of that peak represents the enthalpy change associated with that crystallization process. Finally, the melting transition is characterized by the breadth of the melting process, which includes the onset of melting, the melting temperature taken at the peak in the melting endotherm, and the heat of fusion obtained from the area of the melting endotherm.

Differential scanning calorimetry has a few potential pitfalls which may be avoided. The location and behavior of the transitions detected are sensitive to

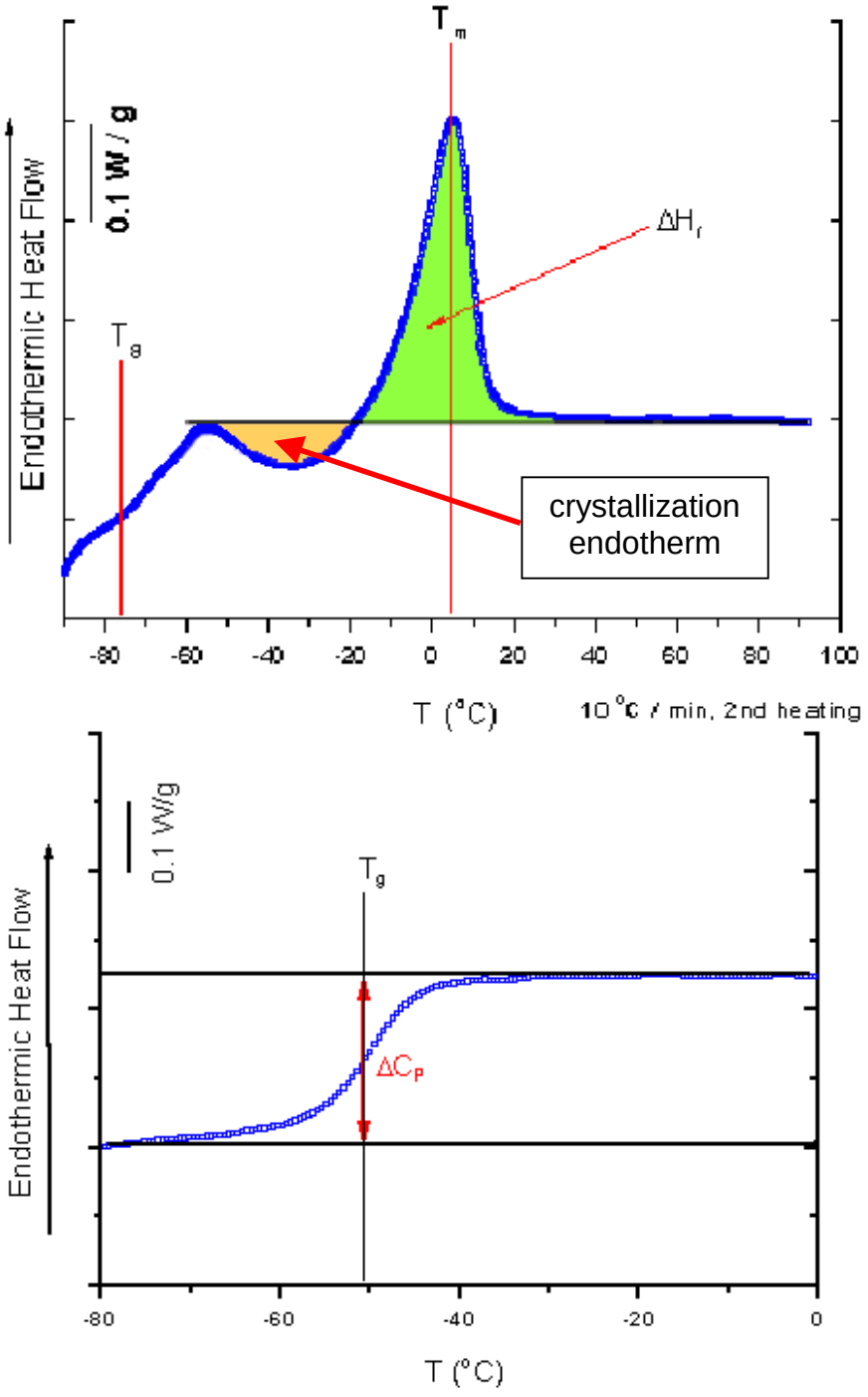

Figure 2-36. DSC scans and information obtained from them.

the experimental heating rate, the thermal history of the sample, and the processing history of the sample. The location and behavior of the transition being investigated will differ depending on the heating rate. It is therefore

important to maintain the same heating rate when comparing results. As a general rule within the present work, a heating rate of 10ºC/min is used. The processing and thermal background of a material may result in morphological features of the polymer that affect the DSC results. Heating the polymer may very well change those features, so it is important to obtain the data from the first DSC heating run as well as subsequent runs. This is particularly true for fibers that can potentially retain orientation information from the fiber spinning manufacturing process.[111] The first DSC heating scan will provide the greatest insight into the effects associated with the thermal and mechanical background (processing) of the material being studied, while the second and subsequent heating scans will reflect more greatly those aspects of the polymer intrinsic to its chemistry and composition. Good contact should be made between the sample and the sample container, typically a small aluminum pan and lid, such that good heat transfer from the instrument to the sample is obtained. This is generally not an issue with film samples, but may be more of an issue when testing fibers and foams.[111] It should be noted, that heat transfer artifacts may occur if a strained sample changes its area of contact with the sample pan.

Section 2-11: Methods – Thermogravimetric analysis

Investigation into the thermal degradation properties of the poly(urethane-urea)s encountered in this study was of secondary focus and will be treated according in this terse review. It was noted in the review of dynamic mechanical analysis that one of the limiting aspects of the technique was its requirement that the sample specimen maintain its physical integrity over the range of temperatures encountered in the experiment. Since the segmented copolymer materials are dependent upon physical crosslinks rather than covalent crosslinks, any softening of the hard domains diminishes the network, and hence the elastomeric nature of the materials. Therefore, dynamic mechanical analysis is not well suited for thermal degradation studies of the poly(urethane-urea)s. Thermal degradation may involve chemical reaction processes such as the scission or crosslinking of the polymer chains. Differential scanning calorimetry is a useful tool for monitoring chemical reactions through the heat consumed or released by the reaction. These heat flows are apparent, respectively, as endo- or exotherms in the DSC scans. However, when thermal degradation of polymers occur, there is often the release of volatile degradation products which may be lost to the atmosphere, complicating DSC analysis. A better method for quantifying the thermal degradation of polymers exists in thermogravimetric analysis, which takes advantage of this tendency to create volatile degradation products. Thermogravimetric analysis (TGA) is a tool in which the weight of a sample is continuously monitored as temperature is elevated.[106-107,112] The transitions monitored with DSC and DMA do not result in weight changes, and

are thus for not registered by thermogravimetric analysis. Therefore, the few thermal degradation studies of the present work, were conducted with TGA. An important feature of these experiments is the choice of atmosphere, which is often the choice between an inert gas, oxygen, or air. Within this study, breathing air is always chosen as the degradation atmosphere.

Section 2-12: Methods – Wide angle x-ray scattering

Differential scanning calorimetry and dynamic mechanical analysis are both capable of detecting cold crystallization processes, and the crystalline content (DSC) of semi-crystalline samples. However, neither is an appropriate tool to detect the onset point of strain-induced crystallization as a function of strain. Recalling some of the earlier comments regarding the different polyols being used for soft segments, only the poly(tetramethylene ether glycol) is crystallizable. Thus, strain-induced crystallization and cold crystallization features are only of interest in PTMEG containing materials. These materials include, poly(urethane-urea)s made with PTMEG and/or blends of PTMEG and PPG soft segments, and blends of poly(urethane-urea)s synthesized from different soft segments. The scale length of the crystal unit cell is considerably smaller than the microphase separated features investigated with small angle x-ray scattering.[113] Recalling Bragg's Law, it was seen that smaller objects scatter radiation at larger angles, and it follows that wide angle x-ray scattering becomes an appropriate tool to detect strain-induced crystallites. Wide angle x-ray scattering may also detect the presence of amorphous ordering in oriented systems, though this is difficult to quantify.[82] All wide angle x-ray studies were performed through a direct film exposure method in which the radiation scattered from crystallites interacts with film. The beam scattered by oriented crystallites exposes the film in such a manner that darkened spots result while oriented amorphous material will appear as a uniform ring or halo (Figures 2-37a and 2-37b). By extending samples in a stepwise fashion, it is possible to approximately

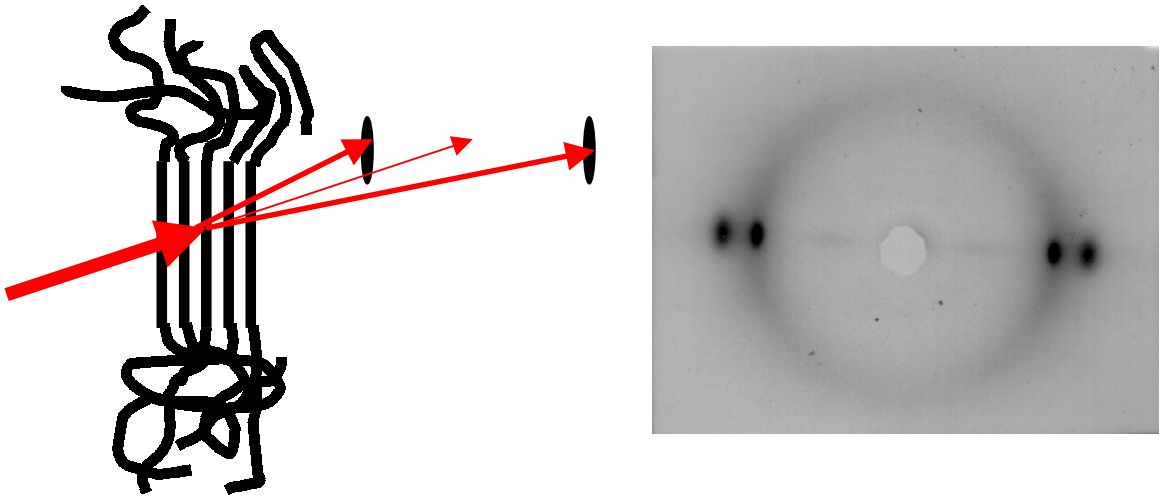

Figure 2-37. Schematic and example of wide angle x-ray scattering for PTMEG crystallites in a vertically oriented PTMEG containing poly(urethane-urea) film material.

determine the extension corresponding to the onset of strain-induced crystallization. Through this procedure, an understanding of the latent crystallizability as a function of composition may be obtained. However, kinetic aspects are lost since the strain rate is not well controlled and it is impossible using available instrumentation to obtain useful instantaneous WAXS images.

Section 2-13: Methods - Birefringence

The remaining methods of poly(urethane-urea) characterization involve a tracking of the orientation behavior of the polymers as they undergo deformation. Two methods are used in this work. The first method is the measurement of birefringence, which provides insight into the system average orientation of all portions of the polymer molecules undergoing deformation. The measurement of infrared linear dichroism is the second method. It is the only method available that probes the orientation behavior of individual segments of these multiblock copolymers.

Since both methods attempt to quantify orientation, whether system average or segmental, it is useful to briefly review what is meant by orientation and specifically Hermans' orientation function (Equation 2-24), which is presented here without derivation.[114-116] The Hermans' orientation function

$$f_H = f = \frac{\left(3\left\langle \cos^2\theta \right\rangle - 1\right)}{2} \qquad (2\text{-}24)$$

where,
f_H is the Hermans orientation function,
θ is the angle of the polymer backbone to a reference axis,
and
f_H = 1 for perfect orientation in the reference direction,
f_H = -1/2 for perfect orientation perpendicular to the reference direction,
f_H = 0 for completely random orientation.

describes the orientation of an element with respect to the deformation direction (Figure 2-38). When the element is aligned parallel to the stretch direction, i.e. at an angle of zero degrees to the stretch direction, the orientation function takes on a value of one. When the element is aligned perpendicular to the stretch

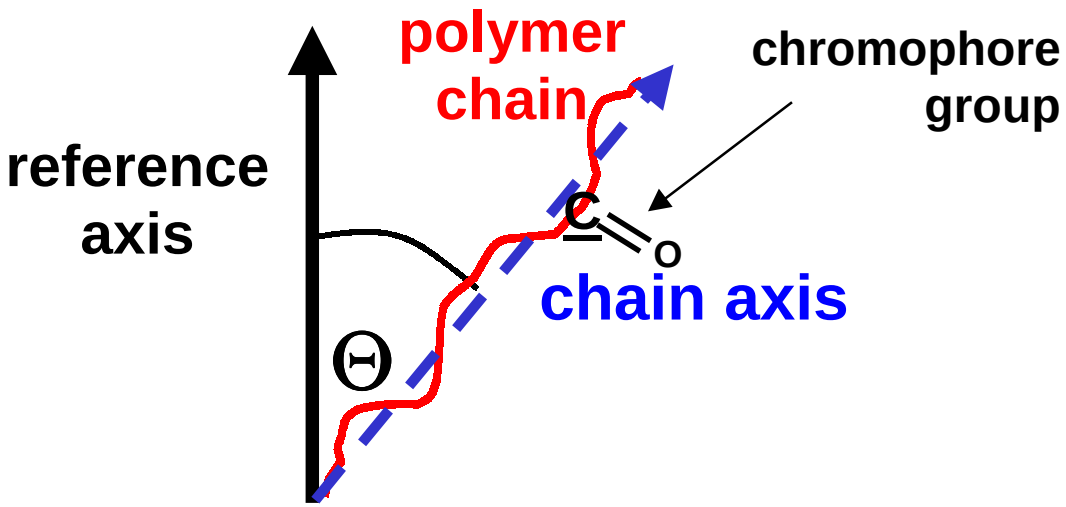

Figure 2-38. Orientation of a polymer chain with respect to a reference axis.

direction, i.e. at an angle of ninety degrees to the stretch direction, the orientation function takes on a value of negative one half. No orientation corresponds to a value of zero. Graphically, the behavior of the orientation function is shown in Figure 2-39. The techniques of birefringence and linear dichroism provide measures of orientation in terms of the described orientation function.

Birefringence, or double refraction, describes the situation which occurs when the refractive indices of two orthogonal directions are not equal.[117] This difference between these two refractive indices is known as the birefringence, Δ_{ij}, (Equation 2-25) and may with some effort be related to the orientation function.[118]

$$\Delta_{ij} = n_i - n_j \qquad (2\text{-}25)$$

where,
Δ_{ij} is the birefringence,
n_i is the refractive index in the i direction, and
n_j is the refractive index in the j direction.

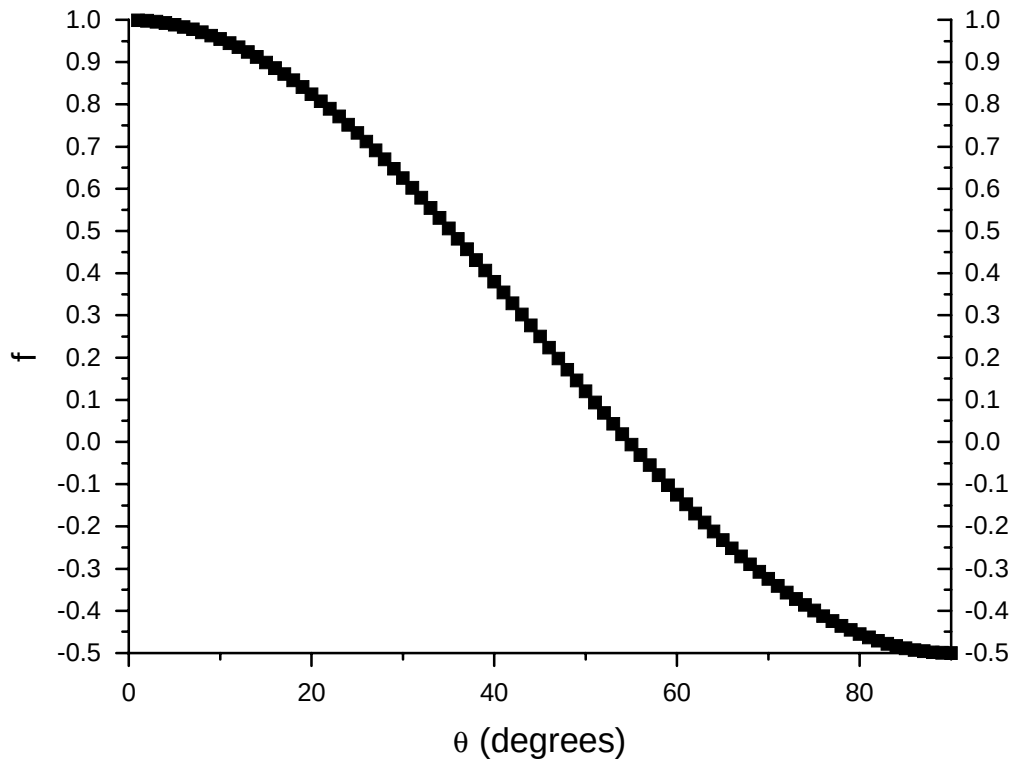

Figure 2-39. Hermans' orientation function, f, as function of the angle, θ, that the polymer makes with respect to a reference direction.

In this study, a compensator method was used to determine the optical retardation, R, which is related to the birefringence (Equation 2-26). The

$$R = d\Delta / \lambda \qquad (2\text{-}26)$$

where,
d is the thickness of the sample,
λ is the wavelength of light used in the study.

directional nomenclature (i.e. i and j) has been omitted for simplicity. The birefringence is proportional to the orientation through a material constant known as the intrinsic birefringence, which is the birefringence for a perfectly oriented sample (Equation 2-27). Without knowing the values of Δ^o for a given poly(urethane-urea) formulation, it is impossible to directly obtain the orientation, but as can be seen, the orientation directly scales with the birefringence for a

$$\Delta = \Delta^o f \quad (2\text{-}27)$$

where,
Δ^o is the intrinsic birefringence,
f is the orientation function.

single phase system. Similarly, birefringence is incapable of separating the orientation due to hard and soft segments without knowing the intrinsic birefringences for each segment, Δ^o_i, as well as the volume fraction of each phase, ϕ_i (Equation 2-28). That is, the observed birefringence, Δ, does not provide the means of determining the separate orientation functions, f_{HS} and f_{ss} for respective hard and soft segments (Equation 2-29). It also does not provide

$$\Delta = \Sigma \phi_i \Delta^o_i f_i \quad (2\text{-}28)$$

$$\Delta = \phi_{HS} \Delta^o_{HS} f_{HS} + \phi_{SS} \Delta^o_{SS} f_{SS} \quad (2\text{-}29)$$

where,
ϕ_i is the volume fraction of ith
Δ^o_i is the intrinsic birefringence of ith
HS is indicative of the hard
SS is indicative of the soft
f_i is the orientation function of ith

a means of distinguishing between the birefringence contributions of mixed soft segment types, such as the case when the poly(urethane-urea) is fabricated with a mixture of poly(propylene glycol) and poly(tetramethylene ether glycol). What's more, the birefringences of materials based upon PPG are not directly comparable to those based upon PTMEG due to the inherent difference in the optical anisotropies of each soft segment type (Chapter 2-3, Figure 2-13). Additionally, poly(tetramethylene ether glycol) has the potential to crystallize, and as mentioned in the discussion of wide angle x-ray scattering, when the temperature and orientation are sufficient, does so upon deformation. When

crystallization occurs, the optical properties of the polymer change, further complicating the analysis. Thus, birefringence will be mostly used when poly(urethane-urea)s based upon PPG are studied systematically as a function of soft segment molecular weight.

Section 2-13: Methods – Infrared linear dichroism

The final method used for the characterization of the poly(urethane-urea)s is infrared linear dichroism. Linear dichroism, whether infrared or otherwise, is simply the property of materials to preferentially absorb radiation that is plane polarized in one direction in contrast to radiation that is plane polarized orthogonally to the first direction.[119] This is somewhat more clear when a reference axis is defined, say the direction or axis of deformation. Materials are said to exhibit orientational dichroism when the material absorbs light polarized parallel to the reference axis preferentially to this same radiation polarized perpendicular to the reference axis, and vice versa. Fourier transform infrared spectroscopy in the near infrared region (400-4000 cm^{-1}) provides a unique avenue for analyzing the segmental behavior of polymers upon deformation. Within this region are many bands uniquely identified with a variety of vibrations associated with the chemical linkages found in organic polymers, such as the stretching of an ether linkage in the backbone of a polymer.[114,119] Considerable work has been conducted by other researchers to identify the origins of these infrared absorption bands, as well as develop an understanding of the molecular geometry associated with each linkage.[48-59,114] Within the field of linear segmented poly(urethane)s and poly(urethane-urea)s there has been extensive study of both the segmental orientation upon deformation and the hydrogen bonding behavior.[48-59,114] While interesting, characterization of hydrogen bonding is not part of the present work. A discussion of the characterization of segmental orientation follows.

Chromophores (e.g. carbonyl in Figure 2-38) along a polymer chain will absorb parallel and perpendicularly polarized infrared radiation to different extents dependent upon the orientation of that transition moment, μ, with respect to the electric vector of the linearly polarized infrared radiation. Knowledge of how those groups geometrically relate to the orientation of the polymer chain allows one to determine the orientation of that portion of the chain.

The absorbances, $A_{||}$ and $A_{\perp}$, are recorded for the cases when the IR radiation is polarized parallel and perpendicular to the reference axis which is generally taken to be the direction of deformation. The ratio of the parallel absorbance to the perpendicular absorbance is known as the dichroic ratio (Equation 2-30). A corrective term for the transition moment associated with the

$$D = A_{||} / A_{\perp} \qquad (2\text{-}30)$$

where,
A is the absorbance,
|| indicates polarization parallel to the deformation axis,
$\perp$ indicates polarization perpendicular to the deformation axis.

specific absorption of the chromophore, D_0, (Equation 2-31) enables one to obtain the orientation function for the chain segment associated with the given chromophore (e.g. the ether linkage or methylene groups will give the orientation for soft segment, while the urea carbonyls can provide the orientation for the hard segments). Finally, through some manipulation, the orientation function may be

$$D_o = 2 \cot^2\alpha \qquad (2\text{-}31)$$

where,
α is the angle of the transition moment to the polymer chain axis.

expressed in a form appropriate to the measured and calculated variables used in linear dichroism (Equation 2-32).

$$f = \left(\frac{D_o + 2}{D_o - 1}\right)\left(\frac{D - 1}{D + 2}\right) \qquad (2\text{-}32)$$

where,
D is the dichroic ratio,
D_o is a geometric corrective factor,
f is the orientation function.

As with any experimental method, there are also limitations to linear dichroism. First, for quantitative work, there must be sufficient signal or transmission of the infrared beam. It is desired that the absorbance associated with a given chromophere be unity or less. Absorbance (or conversely, transmission) is a function of film thickness, chromophore density, and an extinction coefficient which describes the extent to which a given chromophore absorbs radiation of a given wavelength. The materials used in these studies, are predominantly composed of soft segment material. Considering that absorption is the product of thickness, chromophore concentration, and extinction coefficient, it is then required that very thin films (less than 1 mil) must be used to achieve acceptable signal transmission for characterization of the orientation of soft segments. Also, there are often many overlapping bands in the neighborhood of the relevant soft segment absorbance bands which complicates the analysis. Conversely, when films of sufficient thinness for soft segment orientation analysis were used, the absorbances associated with the hard segments were very low, giving a high noise to signal ratio.

Section 2-14: Chapter 2 References

1. Simons DM, Verbanc JJ, J. Polym. Sci 1960; 44: 303.

2. Gee G, Higginson WCE, Taylor KJ, Trenholm HW, J. Chem. Soc. 1961; 4298.

3. Snyder WH, Taylor KJ, Chu NS, Price CC, Trans. N.Y. Acad. Sci. Ser. II 1962; 24: 341.

4. Seneker SD, Barksby N, Lawrey BD, Presented at SPI Polyurethnanes-Las Vegas 1996., Barksby N, Seneker SD, Allen GL, Presented at Fall PMA Meeting-Pittsburgh 1995.

5. U.S. Patent 3,278,457, General Tire Corp. 1966.

6. Herold RJ, Macromol. Syn. 1974; 5:9.

7. Herold RJ, Linigim RA, Polymerization Kinetics and Technology, Advances in Chemistry Series No. 128, American Chemical Society 1973.

8. Barksby N, Seneker SD, Allen GL, Presented at Fall PMA Meeting-Pittsburgh 1995.

9. Hwang KKS, Lin SB, Tsay SY, Cooper SL, Polymer 1984; 25: 948.

10. Zharkov VV, Strikovsky AG, Verteletskaya TE, Polymer 1993; 34: 938.

11. Ning L, De-Ning W, Sheng-Kang Y, Macromolecules 1997; 30: 4405.

12. Ning L, De-Ning W, Sheng-Kang Y, Polymer 1996; 37: 3045.

13. Takahara A, Tashita J, Kajiyama T, Takayanagi M, MacKnight WJ, Polymer 1985; 26: 978., b) Takahara A, Tashita J, Kajiyama T, Takayanagi M, MacKnight WJ, Polymer 1985; 26: 988.

14. Leung LM, Koberstein JT, Macromolecules 1986; 19: 706

15. Sun XD, Sung CSP, Macromolecules 1996; 29: 3198.

16. Rosen SL, Fundamental Principles of Polymeric Materials, John Wiley & Sons, New York 1993.

17. Ultee AJ, in “Manmade Fibers: Their Origin and Development” Seymour RB, Porter RS eds., Elsevier Appl Sci Publ: New York, 1993.

18. Slomkowski S, Winnik MA, Furlong P, Reynolds WF, Macromolecules 1989; 22:503.

19. Croucher TG, Wetton RE, Polymer 1976; 17: 205.

20. McCarthy BJ, Hogen-Esch TE, Macromolecules 1996; 29: 3035.

21. Shirasaka H, Inoue S, Asai K, Okamoto H, Macromolecules 2000; 33: 2776.

22. Vilensky VA, Lipatov YS, Polymer 1994; 14: 3069

23. Sung CSP, Hu CB, Wu CS, Macromolecules 1980; 13: 111.

24. Tyagi D, McGrath JE, Wilkes GL, Polym. Eng. Sci. 1986; 26: 1371.

25. Ophir , Wilkes GL, J. Polym. Sci., Polym. Phys. 1980; 18: 1469.

26. Rosen SL, Fundamental Principles of Polymeric Materials, John Wiley & Sons, New York 1993.

27. Prausnitz JM, Lichtenthaler RN, Azevedo EG, Molecular Thermodynamics of Fluid-Phase Equilibria 2nd Ed. Prentice Hall, Englewood Cliffs NJ 1986.

28. Rosen SL, Fundamental Principles of Polymeric Materials, John Wiley & Sons, New York 1993.

29. Prausnitz JM, Lichtenthaler RN, Azevedo EG, Molecular Thermodynamics of Fluid-Phase Equilibria 2nd Ed. Prentice Hall, Englewood Cliffs NJ 1986.

30. Sperling LH, Introduction to Physical Polymer Science, John Wiley & Sons, New York 1992.

31. Mieczkowski R, Eur. Polym. J. 1991; 27: 377.

32. Mieczkowksi R, Eur. Polym. J. 1992; 28: 53.

33. Hansen CM, Ind. Eng. Chem. Prod. Res. Dev. 1969; 8: 2.

34. Holten-Anderson J, Rasmussen P, Fredenslund A, Ind. Eng. Chem. Res. 1987; 26: 1382.

35. Noshay A, McGrath JE, Block Copolymers, Academic Press, New York 1977.

1. a) Noshay A, McGrath JE, Block Copolymers, Academic Press, New York 1977. States that the difference ought not be large, b) Rosen SL,

Fundamental Principles of Polymeric Materials, John Wiley & Sons, New York 1993. States that $|\Delta_{12}| < 1$ $(cal/cm^3)^{1/2}$ for solubility.

37. Petrovic ZS, Budinski-Simendic J, Rubber Chem. Tech. 1985; 58: 685.

38. Petrovic ZS, Javni I, J. Polym. Sci. B: Polym Phys. 1989; 27:545.

39. Feng D, Venkateshwaran LN, Wilkes GL, Leir CM, Stark JE, J. Appl. Polym Sci. 1989; 37: 1549.

40. Neumuller W, Bonart R, J. Macromol. Sci. B: Phys. 1982; 21: 203.

41. Koberstein JT, Stein RS, J. Polym Sci.: Polym. Phys. 1983; 21: 1439.

42. Arnold RL, Rader CP, "Thermoplastic Elastomers" in Handbook of Plastics, Elastomers, and Composites, Ed. Harper CA, McGraw Hill, New York 1992.

43. Zhao Y, Macromolecules 1992; 25: 4705.

44. Abouzahr S, Wilkes GL, "Segmented Copolymers with Emphasis on Segmented Polyurethanes" in Processing, Structure and Properties of Block Copolymers, Ed. Folkes MJ, Elsevier Applied Science, London 1985.

45. Communication with Dr. J. P. Wightman, Virginia Polytechnic Institute & State University, 1998.

46. Cooper SL, Tabolsky AV, J. Appl. Polym. Sci. 1966; 10: 1837. and Schollenberger CS. U.S. Patent 2,871,218 1959.

47. Garrett JT, Runt J, Lin JS. Macromolecules 2000; 33 (17), 6353.

48. Coleman MM, Skrovanek DJ, Hu J, Painter PC, Macromolecules 1988; 21: 59.

49. Coleman MM, Lee KH, Skrovanek DJ, Painter PC, Macromolecules 1986; 19: 2150.

50. Ning L, De-Ning W, Sheng-Kang Y, Macromolecules 1997; 30:4405.

51. Ning L, De-Ning W, Sheng-Kang Y, Polymer 1996; 37: 3045.

52. Ning L, De-Ning W, Sheng-Kang Y, Polymer 1996; 37: 3577

53. Sung CSP, Schneider NS, Macromolecules 1977; 10:452.

54. Sung CSP, Smith TW, Sung NH, Macromolecules 1980; 13: 117.

55. Estes GM, Seymour RW, Cooper SL, Macromolecules 1971; 4: 452.

56. Brunette CM, Hsu SL, MacKnight WJ, Macromolecules 1982; 15: 71.

57. Takahara A, Tashita J, Kajiyama T, Takayanagi M, MacKnight WJ, Polymer 1985; 26: 978.

58. Takahara A, Tashita J, Kajiyama T, Takayanagi M, MacKnight WJ, Polymer 1985; 26: 988.

59. Senich GA, MacKnight WJ, Macromolecules 1980; 13: 106.

60. Ning L, De-Ning W, Sheng-Kang Y, Polymer 1996; 37: 3577.

61. Bonart R, Morbitzer L, Muller EH, J. Macromol. Sci B: Phys. 1974; 9: 447.

62. Ishihara H, Kimura I, Saito K, Ono H, J. Macromol. Sci. B: Phys. 1974; 10: 591.

63. Ishihara H, J. Macromol. Sci. B: Phys. 1983; 22: 763.

64. Hepburn C, Urethane Elastomers, Elsevier Applied Science, London 1992.

65. Weiss GHR, Natural Rubber Technology 1979; 10: 80.

66. Wittbecker EL, Houtz RC, Watkins WW, Ind Eng Chem 1948; 40: 875.

67. Snyder MD, U.S. Patents 2,623,031 & 2,623,033 (1950).

68. Edgar OB, Hill R, J Polym Sci 1952; 8: 1.

69. Bayer O, Angew Chem 1947; 59: 257.

70. Oertel H, Rinke H, Thoma W, Ger. Patent 1,123,467 (1960).

71. Toyo Spinning Co, Jap. Patent Appl 14,673 (1961) & 12,858 (1964).

72. Wang CB, Cooper SL, Macromolecules 1983; 16: 775.

73. Bonart R, J Macromol Sci-Phys 1968; B2: 115

74. a)1998 DuPont Annual Report and Data Sheet, b) http://www.dupont.com/lycra/facts/fr_history.html

75. Zang YH, Carreau PJ. J. App Polym Sci 1991; 42: 1965.

76. Pope A, An Essay on Man – 1733, from Oxford Dictionary of Quotations, 3rd Edition, Oxford University Press 1979.

77. Li C, Cooper SL, Polymer 1990; 31: 3.

78. Simmons D, Hyperion, Doubleday, New York 1989.

79. Glatter O, Kratky O Eds., Small Angle X-ray Scattering, Academic Press, London 1982.

80. Brumberger H Ed., Small-Angle X-Ray Scattering, Gordon and Breach, New York, 1967.

81. Agarwal BK, X-Ray Spectroscopy: An Introduction, Springer-Verlag, Berlin 1979.

82. Guinier A, Dexter DL, X-Ray Studies of Materials, John Wiley & Sons, New York 1963.

83. Tyagi D, PhD Dissertation, Virginia Polytechnic Institute & State University, Department of Chemical Engineering,1985.

84. Porod G, Chapter 2 in Small Angle X-ray Scattering, Glatter O, Kratky O Eds., Academic Press, London 1982.

85. Vonk CG, in Small Angle X-ray Scattering, Glatter O, Kratky O Eds., Academic Press, London 1982.

86. a) Tyagi D, PhD Dissertation, Virginia Polytechnic Institute & State University, Department of Chemical Engineering,1985. b) Communication with Dr. GL Wilkes 1998.

87. Koberstein JT, Stein RS, J. Polym. Sci: Polym. Phys. 1983; 21: 1439.

88. Koberstain JT, Morra B, Stein RS, J. Appl. Cryst. 1980; 13: 34.

89. Kratky O, Chapter 6 in Small Angle X-ray Scattering, Glatter O, Kratky O Eds., Academic Press, London 1982..

90. Glatter O, in Small Angle X-ray Scattering, Glatter O, Kratky O Eds., Academic Press, London 1982.

91. Luzzati V, Acta. Cryst. 1960; 13: 939.

92. Kratky O, Pilz I, Schmitz PJ, J. Coll. Int. Sci 1966; 21: 24.

93. Pilz I, J. Coll. Int. Sci. 1969; 30: 140.

94. Pilz I, Kratky O, J. Coll. Int. Sci. 1967; 24: 211..

95. Bonart R, Muller EH, J. Macromol. Sci. Phys., 1974; 10: 177.

96. Ruland W, J. Appl. Cryst. 1971; 4: 70.

97. Vonk CG, J. Appl. Cryst. 1973; 6: 81.

98. a) Atkins PW, Physical Chemistry, W. H. Freeman, San Francisco, 1982., b) Giancoli DC, Physics, Prentice-Hall, Englewood Cliffs, NJ 1985.

99. Koberstein JT, Stein RS, J. Polym. Sci.: Polym. Phys. 1983; 21: 2181.

100. Guinier A, Fournet G, Small Angle Scattering of X-Rays, John Wiley & Sons, London 1955.

101. Todo A, Uno H, Miyoshi K, Hashimoto T, Kawai H, Polym. Eng. Sci. 1977; 17: 587.

102. Digital Instruments Online Application Notes, 2/22/00 http://www.di.com/appnotes/AmLab/AL-SPMMain.html

103. Digital Instruments Online Application Notes, 2/22/00 http://www.di.com/appnotes/TapMode/TapModeMain.html

104. Digital Instruments Online Application Notes, 9/7/99 http://www.di.com/appnotes/Phase/PhaseMain.html

105. Digital Instruments Online Application Notes, 2/22/00 http://www.di.com/appnotes/AmLab/AL-SPMMain.html

106. Aklonis JJ, MacKnight WJ, Introduction to Polymer Viscoelasticity, John Wiley & Sons, New York 1983.

107. Sperling LH, Introduction to Physical Polymer Science, John Wiley & Sons, New York, 1992.

108. Gallagher PK in Thermal Characterization of Polymeric Materials, Turi EA Ed., Academic Press, San Diego, 1997.

109. Kajiyama T, MacKnight WJ, Macromolecules1969; 2: 254.

110. Sircar AK, in Thermal Characterization of Polymeric Materials, Turi EA Ed., Academic Press, San Diego, 1997.

111. Rudd GE, in Handbook of Plastics, Elastomers, and Composites, Harper CA Ed., McGraw Hill, New York 1992.

112. Jaffe M, Menczel JD, Bessey WE, in Thermal Characterization of Polymeric Materials, Turi EA Ed., Academic Press, San Diego, 1997.

113. Sircar AK, in Thermal Characterization of Polymeric Materials, Turi EA Ed., Academic Press, San Diego, 1997.

114. Sawyer LC, Grubb DT, Polymer Microscopy, Chapman and Hall, London 1984.

115. Ishihara H, Kimura I, Saito K, Ono H, J. Macromol. Sci. B: Phys. 1974; 10: 591.

116. Zhao Y, Macromolecules 1992; 25: 4705.

117. Jasse B, Koenig JL, J. Macromol. Sci. C: Rev. Macromol. Chem. 1979; 17: 61.

118. Giancoli DC, Physics, Prentice-Hall, Englewood Cliffs, NJ 1985.

119. Lecture Notes of GL Wilkes, Rheo-Optics of Polymers course, Virginia Polytechnic Institute & State University.

120. Jasse B, Koenig JL, J. Macromol. Sci. C: Rev. Macromol. Chem. 1979; 17: 61.

121. Kakuda M, Kasai N, X-Ray Diffraction of Polymers, Kodansha Ltd & Elsevier Publishing Co., New York 1972.